

Strategies for electric vehicle bidding in the German frequency containment and restoration reserves market

Mingyu Seo, Yuwei Jin, Musu Kim, Hyeongyu Son, **Sekyung Han***

School of Electronic and Electrical Engineering, Kyungpook National University, Daegu, 41566, Republic of Korea



ARTICLE INFO

Keywords:
Bidding strategy
Decision-making
Electric vehicle
Optimization scalability
Balancing market

ABSTRACT

Germany's transition to renewable energy sources for a sustainable future has introduced variability and instability in the national power grid, thus necessitating innovative solutions to ensure grid stability and reliable energy supply. The integration of electric vehicles (EVs) in the German balancing market, notably within the frequency containment reserve and automatic frequency restoration reserve sectors, is a potential stabilizing force. However, the complexity of this integration, governed by specific rules in the German energy sector, has not been fully explored. To bridge this gap, a robust schedule that maximizes the economic viability and reliability of EV integration by considering critical elements such as uniform product size, alignment with local market product duration, and customer baseline load is proposed in this study. Mixed-integer linear programming is used for the effective integration of EVs in the German balancing market. This framework emphasizes computational efficiency, providing market participants with precise insights into EV behavior and strategies for energy storage optimization. The effectiveness and reliability of the proposed method are substantiated through case studies. The proposed method consistently achieved maximum profit and a significant reduction in the number of failed cases, which underscores its applicability in real-world scenarios.

1. Introduction

To address global warming and promote environmental sustainability, a shift from traditional power plants to renewable energy sources is critical [1]. Germany, for instance, has been politically committed to phasing out both nuclear and coal power plants. With the declining use of traditional power plants, alternative energy solutions must be devised to ensure electrical grid stability. To facilitate this transition, Europe has adopted several regulations and network codes to promote market integration and resolve power generation inefficiencies [2]. A major step in this direction was the establishment of the European Union (EU)'s Electricity Balancing Guideline (EBGL) in November 2017, which established the foundation for unified European balancing markets [3]. Europe's energy landscape is being reshaped by the regulations that harmonize energy markets across countries, and transmission system operators (TSOs) have collaborated with several energy sectors to overcome the challenges of this transition. Essential services, such as primary frequency control, will be offered via specialized markets using a range of resources—from traditional power plants [4] and demand management systems [5] to energy storage systems (ESSs) [6] and

electric vehicles (EVs) [7]. A central theme emerging from this evolution is the need for co-optimization, which ensures that resources are allocated efficiently across various energy and ancillary service markets, maximizing grid reliability and minimizing system costs. Co-optimization promotes the simultaneous optimization of different services, such as energy, spinning reserves, and nonspinning reserves. The recent EU energy package has highlighted the principle of co-optimization, offering detailed guidelines on the synergized organization of reserve markets. This package provides a vital foundation for any future research on reserve markets [8]. Short-term energy-only markets are orchestrated either a day in advance or intraday by power exchanges, and TSOs are responsible for balancing markets. European balancing markets and their integration with variable renewable energy sources (RES) have been analyzed in detail in a previous study [9].

With an evolving energy landscape that prioritizes co-optimization and grid stability, dwindling fossil fuel reserves, and increasing environmental concerns, EVs are being widely adopted. The global sales of electric cars exceeded 10 million in 2022, which is anticipated to grow by 35 %, reaching approximately 14 million by the end of 2023 [10]. Such wide EV integration has considerably changed the grid's load profile, introducing substantial and unpredictable demands. In contrast,

* Corresponding author.

E-mail address: skhan@knu.ac.kr (S. Han).

Nomenclature	
Abbreviations: (Energy Sources and Systems)	
RES	Renewable Energy Source
EV	Electric Vehicle
BSS	Battery Storage Systems
ESS	Energy Storage System
Abbreviations: (Balancing and Market Terms)	
EBGL	Electricity Balancing Guideline
FCR	Frequency Containment Reserve
aFRR	Automatic Frequency Restoration Reserve
mFRR	Manual Frequency Restoration Reserve
RR	Replacement Reserves
BC	Balancing Capacity
BE	Balancing Energy
DA	Day-ahead
RT	Real-time
Abbreviations: (Entities and Parties)	
TSO	Transmission System Operators
BRP	Balancing Responsible Party
BSP	Balancing Services Provider
Abbreviations: (Programming and Algorithms)	
MILP	Mixed-Integer Linear Programming
NLP	Nonlinear Programming
CMA-ES	Covariance Matrix Adaption Evolutionary Strategy
Abbreviations: (Battery and Charging)	
SoC	State of Charge
CBL	Customer Baseline Load
DCM	Dynamic Charging Mode
DoD	Depth of discharge
Parameters: (Aggregator Parameters)	
D_{AGG}	Droop of the aggregator, representing its response characteristic
P_{AGG}^o	Initial rated power of the aggregator, as specified by the manufacturer
P_{AGG}^{ref}	Reference powers set for the aggregator, typically used for control purposes
P_{AGG}^*	Adjusted rated power of the aggregator after optimization.
R^*	Adjusted number of registered resources under the aggregator after optimization
\mathbb{R}	Total number of controllable resources registered under the aggregator
Parameters: (Costs and Financial Parameters)	
C_{ESS}	Costs associated with the installation and operation of the ESS
C_{PCS}	Costs attributed to the power conversion system
C_{Batt}	Monetary value associated with the battery component
C_{BOP}	Expenditure related to the balance of the plant
ϕ	Capital recovery factor, used to determine the present value of Capital recovery factor, used to determine the present value offuture costs
$C^{O\&M}$	Annual costs dedicated to operations and maintenance of the ESS.
i_r	The annual interest rate applied to financial calculations
y	Expected lifetime of the ESS, typically provided by the manufacturer
Parameters: (Resource and Battery Parameters)	
D_r	Droop of a specific resource, indicating its response to frequency changes
P_r^o	Original rated power of resource r
P_r^{ref}	Reference powers set for resource r
eff_r	Efficiency of resource r during charge-discharge cycles
SoC_r^{min}	Minimum state-of-charge limit for resource r
SoC_r^{max}	Maximum state-of-charge limit for resource r
SoC_r^{max}	Maximum state-of-charge limit for resource r
SoC_r^{max}	Maximum state-of-charge limit for resource r
SoC_r^{max}	Maximum state-of-charge limit for resource r
N_{cycle}	Maximum number of cycles
δ	One-cycle degradation cost
β	Curve-fitting coefficients
m^{seg}	Slope of segment
N^{seg}	Total number of segments
α	Gap length of segment gap length
Parameters: (Market and Bidding Parameters)	
Δf^{param}	Coefficient representing the frequency droop
T	Total number of time slots in the scheduling horizon for resource r
\mathcal{M}	Configuration of the pools used in scheduling
\mathfrak{S}	Scenarios derived from historical balancing service market operation data
$ACPT_{m,\psi}$	Accepted capacity for a specific slot Ψ in mode m
Variables	
$SoC_{r,t}$	State-of-charge of resource r at a specific time slot t
$init_r$	Initial state-of-charge of resource r when plugged in
SoC_r^{Goal}	Desired state-of-charge for resource r at the end of the scheduling horizon
Δf^*	Actual grid imbalance observed
Ξ	Set of decision variables used in the optimization
$UC_{r,m,t}$	Binary variable indicating the pool allocation of resource r at time slot t in mode m
$UC_{r,m,t}^{bid}$	Binary variable indicating the bidding pool allocation of resource r at time slot t in mode m
$UC_{r,m,t}^{backup}$	Binary variable indicating the backup pool allocation of resource r at time slot t in mode m
$P_{r,m,t}$	Variable representing the bidding capacity and charging power of resource r at time slot t in mode m
$P_{r,m,t}^{bid}$	Bidding capacity of the resources for a specific time slot
$P_{r,m,t}^{backup}$	Resources allocated for backup during a specific time slot
$Bid_{m,\psi}$	Bidding capacity for a specific slot Ψ in mode m
$\tau_{m,t}$	Ratio indicating the volume activated during a specific time slot
$P_{r,m}^{min}$	Minimum power that resource r can provide in mode m
$P_{r,m}^{max}$	Maximum power that resource r can provide in mode m
$\Pi_{m,\psi}$	Consecutive 4-hour bidding periods in mode m
$rate^{backup}$	Rate representing the retention of backup resource capacity
Ψ	Set of available bidding products during the scheduling horizon
seg	Segment index
X_t^{seg}	Binary indicator of the segment

the proliferation of EVs is a promising opportunity for effective demand side management and improved energy market operations [11]. Due to the inherent longer charging times associated with EVs, strategies concerning their optimal use have been devised. Modern EV infrastructure provides sophisticated charging solutions, facilitating both grid-to-vehicle (G2V) and vehicle-to-grid (V2G) operations [12]. However, the limited energy capacity of a single EV is a challenge; this challenge can be addressed using an EV aggregator that is an intermediary among market operators, EV owners, and system administrators [13]. With the integration of EVs in energy systems, their interplay with specialized energy markets must be considered. Their charging and discharging patterns can considerably influence balancing mechanisms, emphasizing the need for a closer examination of these markets.

Energy markets are characterized by a multifaceted landscape. These balancing markets are classified into four categories: the frequency containment reserve (FCR), automatic frequency restoration reserve (aFRR), manual frequency restoration reserve (mFRR), and replacement reserve (RR) [14]. European balancing markets and their pivotal ties to variable RES were comprehensively analyzed previously [15]. From these reserves, control reserves that are differentiated by their immediacy of response are procured by TSOs. For example, the FCR is designed to be fully operational within a mere 30 s, whereas the aFRR is set to activate within 5 min and the mFRR within 15 min after an imbalance event. With the integration of EVs, energy market adaptations must be studied in detail. In these evolving dynamics, the roles of different reserves in the balancing markets must be recognized for effective harmonization with EV load patterns. A shift in the FCR has been observed, influenced by the rise of EVs and ESSs. Nonspinning reserves for FCR are being adopted owing to their rapid power delivery capabilities to meet the increasing demands of EV charging. A 5-minute response window is maintained for aFRR. The mFRR poses challenges due to its longer activation period and substantial power requirements. The integration of nonspinning reserves into the mFRR is complicated by factors such as extended start-up times. However, the needs of mFRR are met primarily by synchronized spinning reserves [16]. Amid these shifts, the significance of TSOs in maintaining grid stability is underscored, particularly with the continued growth of EV adoption.

This study focuses on the FCR and aFRR markets. To participate in the FCR and aFRR market, technical units are required to meet several benchmarks by Regelleistung [17]. The operation of reserve markets can vary based on country-specific regulations and the nature of the reserve. Certain markets might be structured around a single-stage capacity-only model, whereas others might adopt a two-stage model encompassing capacity and activation. Additionally, the choice of the pricing model, be it pay-as-bid or marginal, can differ across markets. A potential transition toward the marginal pricing rule in imminent European platforms designated for FCR and aFRR activation has recently been indicated [18].

The profitability of FCR has been scrutinized using econometric models in a recent study [19], which unveiled a notable positive correlation between grid stability and FCR market growth and emphasized the need to focus on diverse bidding strategies to optimize profitability. A study that compared the aFRR market with different global markets revealed the indispensable role of the aFRR market in maintaining grid balance when energy sectors are increasingly relying on renewable sources [20]. Historical data were analyzed [21] to understand the importance of FCR and aFRR markets in ensuring grid balance. The findings advocated for stakeholders to foster knowledge-sharing collaborations to enhance bidding outcomes. Pavic et al. [7] employed a hybrid methodology comprising qualitative and quantitative approaches to study the FCR and aFRR to realize their full potential. Although mathematical bidding models tailored for the FCR and aFRR markets have been developed [21,22], the integration of crucial practical rules has been overlooked. Moreover, FCR and aFRR markets for EV fleets have not been comprehensively analyzed in the literature.

2. Literature review and contributions

The foundational theories of the German markets for FCR and aFRR are discussed here through a literature review [23]. This review offers holistic insight into the principles and commercial structure of these specific reserve markets within the context of the German energy sector. The intricacies and nuances associated with these markets have been rigorously analyzed previously [24]. The subsequent sections will elucidate the factors considered in this study.

2.1. European balancing markets

European balancing markets are key platforms for monetizing flexible energy generation. Most studies have focused on portfolio optimization related to balancing markets (e.g., [25]). As European countries continue to liberalize market access policies to encompass emerging flexibility resources, scholars have extensively explored the feasibility of distributed energy technologies, such as battery storage [26], heat pumps [27], domestic solar photovoltaic panels combined with storage [28], and the integration of demand response for frequency support [29].

European balancing markets find their origin in the intrinsic requirements of the infrastructure components, characterized by the commitment of TSOs to ensuring energy balance. This balance is crucial for maintaining the requisite network frequency across integrated systems. System imbalances are caused by factors such as stochastic events, predictive uncertainties surrounding load and generation, unpredicted equipment failures, and unpredictable market behaviors. The balancing markets and associated regulatory frameworks are shown in Fig. 1.

The operational sequence of electricity balancing markets begins with an auction process for the reservation of balancing capacity (BC) to ensure sufficient reserves for prospective activation. Then, balancing energy (BE) is actuated in real-time to address systemic deviations by employing the aggregate of balancing resources acquired in the preliminary phase. A post-real-time financial harmonization between the TSO and balancing responsible parties (BRPs) is performed based on the polluter-pays principle. The resultant imbalance prices depend on the financial outlay for BE.

The TSO manages imbalances between electricity production and consumption simultaneously (Fig. 1). From the stakeholders' perspective, the TSO serves as an intermediary between balancing services providers (BSPs) and BRPs, with the latter predominantly responsible for inducing imbalances. In contrast with the day-ahead and intraday markets, only participants who satisfy stringent prequalification standards can function as BSPs. BRPs operate by conglomerating market stakeholders (both electricity producers and consumers), thus optimizing economies of scale. They subsequently convey their anticipated load and generation projections to the TSO a day prior.

The electricity balance guideline (EU Reg. 2017/2195, Nov. 23, Electricity Balance Guideline) provides insights into the regulatory framework and shows how TSOs handle imbalances by procuring balancing services from BSPs prior to real-time operations in the BC marketplace. Real-time system irregularities, such as deficits and surpluses, are caused by frequency variations in the expected network and corrected using the regulatory capacity secured from BSPs. BRPs compensate the TSO for deviations from initial forecasts resulting from the prediction errors of RES. Unlike spot markets, where trading is bidirectional, balancing markets are inherently unidirectional, with the TSO acting as the sole purchaser. The standard balancing products outlined by the EBGL are FCR, aFRR, mFRR, and RR, which have different activation timelines and durations.

This study focuses on German markets; however, as Table 1 shows, the method proposed in this study is scalable within the EU. FCR and aFRR are consistently observed across major European nations, particularly Germany, Finland, and France. These countries were chosen for comparison owing to their diverse energy markets and regulatory

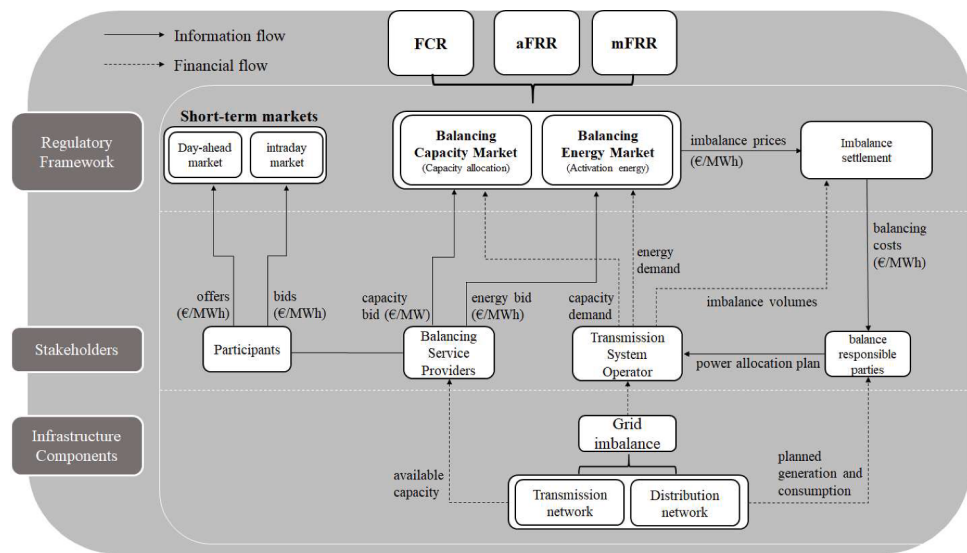


Fig. 1. Organization of the European power balancing market and its connection to the short-term power market [30].

Table 1
Comparative analysis of the FCR and aFRR mechanisms across Germany [31], France [32], and Finland [33].

Country Purpose	FCR			aFRR		
	Germany	France	Finland	Germany	France	Finland
Stabilize frequency	Stabilize frequency	Stabilize frequency	Stabilize frequency	Restore Frequency	Restore frequency	Restore frequency
Response Time	Seconds	Seconds	Seconds	≤5 min	≤10 min	≤3 min
Bidding Window	Day-ahead	Day-ahead	Day-ahead	Day-ahead	Day-ahead	Day-ahead
Settlement Basis	Capacity	Capacity	Capacity & Energy	Capacity	Capacity	Capacity & Energy
Periodicity of Settlement	Weekly/Daily	Daily	Weekly/Daily	Daily	Daily	Daily
Auction Product	Symmetrical (up/down)	Symmetrical (up/down)	Symmetrical (up/down)	Asymmetrical (up or down)	Symmetrical (up or down)	Asymmetrical (up or down)

landscapes, thus providing a holistic view of EU-wide applicability. As shown in Table 1, for FCR, all three countries use “capacity” as the settlement basis, with Finland additionally incorporating “energy.” For aFRR, the settlement basis in all three nations includes “capacity” and “energy.” The periodicity of settlements for FCR is daily in France, whereas Germany and Finland alternate between weekly and daily settlements. All three countries adopt symmetrical products (up/down) for FCR. For aFRR, Germany and Finland use asymmetrical products (either up or down), whereas France uses symmetrical products. Based on these differences, challenges in bidding strategy algorithms are outlined. The unique incorporation of both “capacity” and “energy” for FCR by Finland implies that adjustments akin to those for aFRR are required for the objective function representing FCR bids in Finland. Asymmetric bids for aFRR adopted by Germany and Finland can lead to further complexity; this bidding approach can be tailored based on specific behaviors of either absorbing or discharging energy. Such flexibility is advantageous for resources with unidirectional capabilities but may be challenging for those with bidirectional capabilities such as EVs. The decision to bid for energy absorption, discharge, or both and their capacity allocation is also influenced by market prices, resource constraints, and grid requirements. Nevertheless, these differences are considered minor from a bidding strategy perspective. Although the proposed method focuses on the German market, it can be widely adapted and scaled across Europe with minor modifications.

For FCR, providers are required to deliver a predetermined volume when a frequency deviation exceeds the established deadband of 49.99–50.01 Hz. This automatic and unbiased activation is determined by the frequency observed within the synchronous area. Suppliers

autonomously monitor grid frequency at specified points for power consumption and generation and address frequency deviations immediately. The aFRR is typically activated 30 s after FCR activation. For ensuring grid stability within the Continental Europe.

Synchronous Area, 3000 MW of power must be continuously and equally distributed between positive and negative primary control reserves. This value is equivalent to the combined output of the grid’s two largest power plants [34].

For the FCR, bids that incorporate the BC volume (MW) and the corresponding BC price (€/MW) are submitted. The bids are selected based on a meritocratic ranking system, prioritizing the most competitive offers until the required amount of FCR is covered. These reserves are activated automatically during frequency deviations, and the compensation is based on the bid price and the actual delivery of the FCR service. Similar bids are submitted for the aFRR. The BE activation price (€/MWh) is typically presented during the BC auction, limiting BE provision to only successful BSPs. The BC auction adopts a meritocratic ranking system, followed by a subsequent ranking for the BE market.

Six products are auctioned daily, each for 4 h, and the products are scheduled for deployment on the following day. Fig. 2 depicts this routine, showcasing the bidding dynamics of FCR, aFRR-p, and aFRR-n throughout the day. The tender invitations are consistently dispatched at 8 am (Central European Time). In the auctioning framework, FCRs and aFRRs are procured using symmetrical and asymmetrical bids, respectively. The distinct roles of aFRRs comprising positive (aFRR-p) and negative (aFRR-n) primary reserves in maintaining grid stability are reflected through these bids, wherein providers are mandated to offer equal quantities of both reserves. This approach aligns with the



Fig. 2. Daily FCR and aFRR auction process: six positive and six negative 4 h product segments [26].

symmetrical bidding approach adopted for FCRs. In this phase, all bids are collected and ranked based on merit by the designated TSOs of respective nations. Then, the necessary FCR volume is acquired from the suppliers whose bids are most economically viable. Within this FCR procurement framework, bids are categorized as either divisible or indivisible, with the latter being limited to a maximum of 25 MW across all participants. The aFRRs comprising aFRR-p and aFRR-n primary reserves are procured through asymmetrical bids in which their distinct roles in maintaining grid stability are reflected. These primary reserves are differentiated by their unique responses to grid frequency variations. When the grid frequency decreases below the standard, the aFRR-p is activated to address the detected energy deficit. In contrast, when the grid frequency increases above the standard, the energy surplus is addressed by activating the aFRR-n. The aFRRs and their asymmetrical bidding nature are further elucidated based on the procurement strategy for fulfilling aFRR demand, which is characterized by transparency, pay-as-bid mechanisms, and participant anonymity. However, to be deemed eligible, units must meet stringent criteria [35]. Aligning with the evolving European electricity market regulations, balancing services have transitioned to a market-centric procurement approach [26]. However, the architecture of these balancing markets differs across EU member states [36]. While certain markets require symmetrical bids from BSPs, others permit asymmetrical propositions. The compensation structures can either adopt a pay-as-bid framework or a marginal price model. The fundamental difference between these models is their compensation strategy; the former compensates based on the bid price, whereas the latter utilizes a uniform market-clearing price. Furthermore, balancing products differ based on their activation durations, ranging from an entire day to a mere hour [31].

2.2. Bidding strategies

The reserve market is indispensable for modern energy systems and addresses unexpected demand surges or supply deficits. Battery storage systems (BSSs) have garnered considerable attention owing to their ability to swiftly respond to grid requirements. The intricate relationship between performance-based regulation and battery degradation and the influence of these factors on BSS bidding strategies in the reserve market have been previously investigated [6,37]. Results revealed that these factors enabled BSS operators to formulate bids that increased the profitability and operational life of storage systems, ensuring their sustained presence in the reserve market. The role of battery storage in the European reserve market, particularly the German market, has also been elucidated [26,38,39]. Analysis of the reserve capacity and activation costs revealed that BSS bids can be fine-tuned to guarantee profitability and reliability during high-demand intervals. Further insights into the role of BSSs in the reserve market have also been reported [40,41]. These studies shed light on the delicate balance between bids driven by profit motives and those considering battery lifespan; they also emphasize the significance of performance-based regulation in directing BSS operators to formulate effective bids for the reserve market.

BSSs have successfully addressed the immediate needs of the reserve market; however, EVs have emerged as a promising alternative. EVs, with their substantial battery capacities, are revolutionizing

transportation and emerging as potential contributors to the energy grid, particularly in FCRs and aFRRs [7]. Owing to their excellent battery storage capacities, EVs can be used to manage adaptive loads in the electrical grid. EVs assimilate surplus energy during periods of increased generation and supply it when the demand is high [11]. However, some challenges, such as the unpredictable EV charging patterns and vehicular preparedness for end users, can decrease their dependability as grid assets [42]. Recent research has explored the potential of EVs and their aggregators to address the challenges of the reserve market and revealed that EV aggregators can play a pivotal role in addressing sudden grid demands.

A stochastic and dynamic mixed-integer linear programming (MILP) model tailored for EV aggregator bidding in the reserve market has been previously introduced [43]. Considering the uncertainties in market prices, renewable outputs, and EV behaviors, a strategic framework was provided for aggregators, ensuring that drafted bids are both competitive and responsive to the dynamic needs of the reserve market. The intricacies of EV aggregator bidding strategies for the reserve market have been reported in previous research [21,44,22], which emphasized the importance of real-time adaptability in the reserve market, suggesting that bids must be crafted by aggregators in a manner that is both predictive of grid needs and flexible in adapting to real-time changes. Challenges faced by individual EVs when integrated into the reserve market have also been explored [14]. The aggregator's pivotal role in ensuring that the bids facilitate seamless cooperation between individual EV owners and the system operator has been highlighted, emphasizing the importance of grid stability during peak demand periods. The influence of community-based EV sharing schemes on bidding in the reserve market has been explored from a unique community perspective [45]; results indicated that when communal EV fleets are effectively managed, a reliable energy buffer during peak demand periods can be provided, ensuring grid stability and optimized energy consumption. A critical perspective on the uncertainties inherent in the reserve market was presented by Pavic et al. [7], who evaluated deterministic bidding models and advocated for strategies that inherently incorporate these uncertainties. The dynamic demands of the reserve market can be consistently met by adopting such an approach.

To comprehensively overview the cited studies, a taxonomy was meticulously developed, shown in Table 2, wherein studies were systematically categorized based on their primary focus areas, bidding strategies, mathematical considerations, and optimization techniques. The process of ensuring that each product within a market segment adheres to a standardized capacity is described as “uniform product sizing”. Meanwhile, the notion of customer baseline load (CBL) has been derived from demand response programs. In these programs, a standard measure for a customer's typical electricity consumption is determined, which is used as a foundational reference to gauge any variations in consumption. Section 3 discusses the CBL in detail along with the state of charge (SoC) variance. This aspect evaluated whether existing studies had considered potential fluctuations in SoC, which could emerge from the complexities associated with procurement processes in the reserve market. To the best of our knowledge, bidding strategies considering all practical rules and risks of procurement failures have not been reported yet.

Table 2

Taxonomy of the proposed methodology compared to representative literature studies.

Reference	Focus area	Bidding strategy type				Practical rules considered			Optimization technique
		FCR	aFRR	DA	RT	Uniform product sizing	Customer baseline load	In terms of taking into account of SoC variance	
[6]	ESS		✓		✓			✓	MILP
[37]	ESS		✓	✓				✓	NLP
[26]	ESS	✓			✓				CMA-ES
[38]	ESS		✓		✓	✓		✓	CMA-ES
[39]	ESS		✓		✓			✓	MILP
[40]	ESS	✓		✓				✓	MILP
[41]	ESS	✓			✓			✓	Stochastic Optimization
[43]	EV fleet			✓				✓	stochastic and dynamic MILP
[44]	EV fleet	✓			✓	✓			Genetic algorithms
[22]	EV fleet	✓			✓	✓		✓	Nonlinear Programming
[21]	EV fleet		✓	✓				✓	MILP
[14]	ESS, EV fleet		✓	✓				✓	LP
[45]	EV fleet			✓				✓	Stochastic programming
[7]	EV fleet	✓	✓	✓	✓			✓	Stochastic Optimization
This Paper	EV fleet, ESS	✓	✓	✓	✓	✓		✓	MILP

2.3. Contributions and organization

In this study, significant gaps within the field of multimarket bidding strategies were addressed. Following are the main contributions of this study:

- Development of a comprehensive multimarket bidding strategy: An innovative bidding strategy tailored to multimarket contexts was introduced by incorporating factors such as uniform product sizing and CBL. The augmentation of market efficiency was identified as the primary objective of this strategy, and a holistic method for bidding in diverse market environments was proposed.
- Quantitative representation of bidding parameters: The need for a structured approach was acknowledged, and the bidding rules were transformed into a linear mathematical framework. This quantitative representation provided a clear and systematic way to understand and apply the bidding rules, enhancing computational efficiency. The proposed model can be used with enhanced precision by market participants and stakeholders.
- Risk examination of EV behavior uncertainty: Procurement failures attributable to unpredictable EV behavior were analyzed to provide stakeholders with insights into the associated challenges.
- Optimization strategies for ESS reserves: The auxiliary ESS capacity required to mitigate potential procurement disruptions was calculated. Furthermore, methodologies for streamlining this backup capacity were elucidated, ensuring that mechanisms to cost-effectively maintain system reliability are available.

The remainder of this paper is organized as follows: Section 3 elucidates the mathematical model of the proposed framework. Section 4 verifies the robustness and efficacy of the model based on different scenarios. Section 5 provides a comprehensive analysis of the findings and outlines potential avenues for future research.

3. Methodology

3.1. Proposed framework

The potential for integrating EVs and ESS assets from residential and commercial buildings into the flexibility market is explored in this study. The performance of battery-powered ESS and EVs in FCR and aFRR stabilization is validated. Owing to their quick response, ESSs and EVs are identified as suitable candidates for meeting the immediate demands of the FCR market. The collective response of ESSs and EVs can

effectively address disturbances in the FCR market. Their inherent adaptability and sustained response are also suitable for the aFRR market, which prioritizes restoring grid frequency over long durations. Using EV aggregators, these systems can be integrated feasibly into both markets and will be beneficial to grid stability and efficiency.

The roles of aggregator systems and gateway operators must be defined as they vary across markets. The aggregator, pivotal to the proposed model, manages a diverse pool of resources and undertakes responsibilities such as calculating the serviceable capacity, proposing services to the TSO, and vigilantly overseeing the status of resources. In contrast, the gateway operator acts as the executor and meticulously controls the energy resources based on schedules relayed by the aggregator.

In the aFRR, the gateway operator receives commands from the TSO directly and responds to them during specified timeslots. Resources earmarked for this service are readily available and supplied in response to the specific commands. The aggregator, having crafted the operational scheme, ensures that the resources are aligned for such commands, but their real-time control and adjustments are managed by the gateway operator. The gateway operator's connection to a power meter is integral to the FCR's function. The gateway operator can adjust the output of EVs if the grid frequency deviates from the established deadband, thereby ensuring grid stability. This real-time monitoring and control of energy-resource charge or discharge highlight the gateway operator's crucial role in swiftly meeting the demands of the FCR market.

Fig. 3 shows a droop-based frequency response setting for ESSs, which generates an adaptive power output based on frequency deviations, similar to traditional synchronous generators. Notably, non-spinning reserves, which include energy storage mechanisms, are integral to the FCR. These reserves are ever-alert in tracking frequency variations and taking action based on the set droop characteristics. The deadband of the frequency control mechanism is established at $50 \text{ Hz} \pm 0.01 \text{ Hz}$, and any deviation from this range triggers immediate intervention. The efficacy of frequency-response services is determined based on critical factors such as the deadband, droop coefficient, response speed, and the response duration for is sustained. The droop value can be calculated based on the droop coefficient for appropriating the FCR service as follows:

$$D_{AGG} = \frac{\Delta f^{param}}{P_{AGG}^0} \quad (1)$$

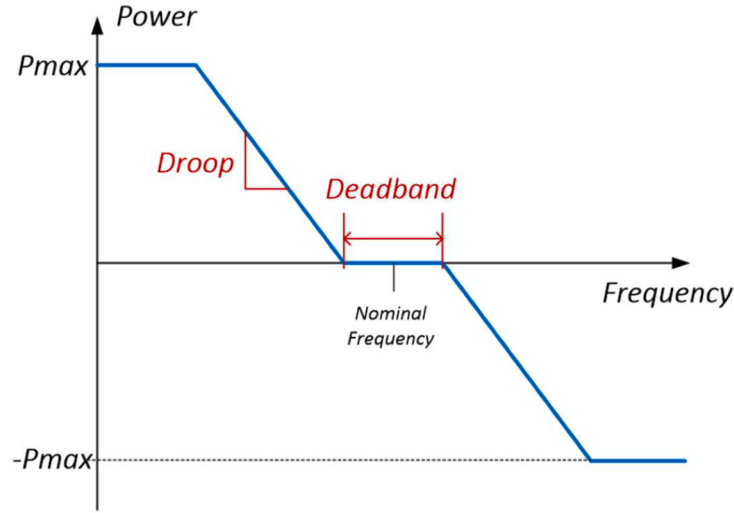


Fig. 3. Droop-based frequency response for energy storage systems [46].

$$P_{AGG}^o = \sum_{\mathbb{R}} P_r^o$$

Hence, the droop, D_r , of each response is

$$D_r = \frac{\Delta f^{param}}{P_r^o}, \quad \forall r \in \mathbb{R} \quad (3)$$

where D_{AGG} is the aggregator droop, Δf^{param} is the frequency droop coefficient of the TSO, P_{AGG}^o is the rated power of the aggregator, which is the sum of the rated power (P_r^o) of the allocated EVs belonging to \mathbb{R} , and D_r is the droop of the resource r of the EV.

When a grid imbalance of Δf^* occurs, the reference powers of the aggregator and allocated EVs are calculated as follows:

$$P_{AGG}^{ref} = \frac{\Delta f^*}{D_{AGG}} \text{ and } P_r^{ref} = \frac{\Delta f^*}{D_r}, \quad \forall r \in \mathbb{R} \quad (4)$$

If an unexpected plug-time change occurs, the D_r is changed to D_r^* as follows:

$$P_{AGG}^* = \sum_{\mathbb{R}^*} P_r^o \quad (5)$$

$$P_r^* = \frac{P_r^o}{P_{AGG}^*} P_{AGG}^*, \quad \forall r \in \mathbb{R}^*$$

The droop, D_r^* , of each resource is renewed:

(2)

$$D_r^* = \frac{\Delta f^{param}}{P_r^*}, \quad \forall r \in \mathbb{R}^* \quad (6)$$

The renewed rated power of the aggregator, P_{AGG}^* , is determined by the sum of the rated powers of the EVs belonging to \mathbb{R} . Even when P_{AGG}^o is updated to P_{AGG}^* , the Δf^{param} remains unchanged. Consequently, an allocation problem arises, leading to changes in the droop of the EVs, as shown in Eqs. (5) and (6).

Herein, the “dynamic charging mode (DCM)” is introduced for EVs in addition to the basic modes. The DCM represents a charging strategy employed by the aggregator to align the SoC with the desired level during operational hours. For instance, if the SoC of an EV is insufficient for participation in the most profitable FCR, charging is initiated to achieve the required SoC, thereby enabling the EV to partake in the FCR during subsequent time slots. Both the EV and ESS operations are dictated by this schedule; the EV is prioritized, and the ESS serves as a backup. If the EV fails to operate as scheduled, the ESS, being a fixed asset, is mobilized to deliver the balancing service. The conceptual framework for the market aggregator and gateway operator is shown in Fig. 4.

During the daily 4 h auction of each product, the aggregator undertakes the following steps:

1. The daily EV schedule is received from the user.
2. The optimal scheduling of the ESS and EV is executed in 1 h increments based on the user-provided schedule (the more profitable

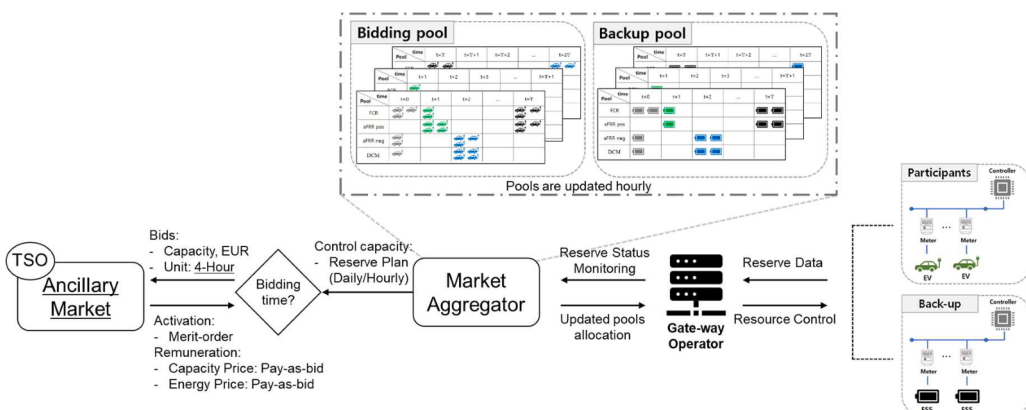


Fig. 4. Proposed framework for market aggregator and gateway operator.

- DCM and balancing services are prioritized during this optimization).
3. For reserve planning, schedules are segmented into consecutive 4 h products.
 4. Bidding and backup pool schedules are relayed to the gateway operator for implementation. However, the actions of the gateway operator are contingent on real-time field conditions.

3.2. Mathematical model

Herein, the mathematical formulation of the aggregator is discussed, using which the serviceable capacity of the bidding pool is calculated. The model is formulated using MILP to address the allocation problem and ensure computational efficiency for practical applications.

The objective function of the proposed model, as presented in Eq. (7), maximizes revenues from balancing service participation by determining the optimal serviceable bidding pool capacity while concurrently minimizing the resource charging cost and battery degradation cost. Market revenue is derived from both BC volume and BC price. The bidding capacity for a given bidding interval ψ in mode m is denoted by $Bid_{m,\psi}$.

Each interval ψ spans 4 h. In Eq. (8), the revenue from the BC volume is calculated by multiplying $Bid_{m,\psi}$ with the unit price of the BC, $CapacityUnitPrice_{m,t}$. Compensation for energy procurement is determined by multiplying the $Bid_{m,\psi}$ with the volume-activated ratio, $\tau_{m,t}$, associated with the balancing services. \mathbb{R} denotes the number of registered controllable resources of the aggregator, including the EV for the bid and ESS as backup. \mathbb{T} represents the total number of time intervals in the scheduling horizon. \mathcal{M} denotes the configuration of the pools in scheduling. In the proposed method, \mathcal{M} encompasses {FCR, aFRR-p, aFRR-n, DCM}, capturing the entire market group within the balancing services and DCM. The decision variable, $P_{r,m,t}$, indicates the bidding capacity for market pools and charging power for the DCM pool of the rth resource at time interval t in mode m. This variable includes $P_{r,m,t}^{bid}$ and $P_{r,m,t}^{backup}$, which are differentiated by the type (use) of resources. As $P_{r,m,t}^{backup}$ acts as a backup resource, it is not included in the bid, ensuring the model's robustness against uncertainties. As a result, it is not factored into the revenue terms.

$$\arg \max_{\Xi} market_{income} - Energy_{cost} - \sum_{\mathbb{R}} \sum_{\mathbb{T}} \sum_{\tilde{s}} b_{r,t}[\tilde{s}], \quad (7)$$

$$\Xi = \left\{ \begin{array}{l} UC_{r,m,t} \ni (UC_{r,m,t}^{bid}, UC_{r,m,t}^{backup}), \\ P_{r,m,t} \ni (P_{r,m,t}^{bid}, P_{r,m,t}^{backup}), \\ Bid_{m,\psi} \end{array} \right\}$$

subject to

$$Market_{income} \quad (8)$$

$$Energy_{cost} \quad (9)$$

Constraints for the proposed model are as follows:

$$\sum_{\mathcal{M}} UC_{r,m,t} \leq 1 \quad (10)$$

$$UC_{r,m,t} \cdot P_{r,m}^{min} \leq P_{r,m,t} \leq UC_{r,m,t} \cdot P_{r,m}^{max} \quad (11)$$

$$SoC_{r,0} = init_r \quad (12)$$

$$SoC_{r,t}[\tilde{s}] = SoC_{r,t-1} + \sum_{\mathcal{M}} \sum_{CSC} \left\{ \frac{P_{r,m,t}}{Q_r} \cdot \tau_{\tilde{s},m,t} \right\} \cdot eff_r + \frac{P_{r,SC,t}}{Q_r} \cdot eff_r$$

$$SoC_r^{min} \leq SoC_{r,t}[\tilde{s}] \leq SoC_r^{max} \quad (13)$$

$$SoC_r^{Goal} \leq SoC_{r,T_r}[\tilde{s}] \quad (14)$$

$$SoC_r^{min} \leq SoC_{r,t}[\tilde{s}] \pm P_{r,FCR,t} \leq SoC_r^{max} \quad (15)$$

In Constraint (10), allocation is regulated to avoid resources provision to multiple modes for the same time slot, t. $UC_{r,m,t}$, a binary decision variable of $\in \{0, 1\}$, indicates the pool allocation of the rth resource at time slot t in mode m.

In Constraint (11), the upper level of the bidding capacity of resource r is established. $P_{r,m,t}$ is bounded by the maximum ($P_{r,m}^{max}$) and minimum ($P_{r,m}^{min}$) available participation power, which is determined by $UC_{r,m,t}$. Thus, flexibility in participation capacity is provided only when resource r is deployed in the pools.

Constraints (12)–(14) are formulated to estimate the SoC based on balancing service participation and DCM in kWh units. The SoC represents the current energy level of a battery or ESS relative to its maximum capacity. $SoC_{r,t}$ denotes the SoC of resource r at time slot t. Each resource, r, is constrained by the minimum (SoC_r^{min}) and maximum (SoC_r^{max}) ranges of the SoC, as detailed in Constraint (13). In Constraint (14), it is ensured that resources maintain an SoC above the target SoC in the final time slot, T_r . $init_r$ is defined as the plug-in SoC of resource r. $\tau_{m,t}$ represents the volume-activated ratio of the balancing service at time slot t in mode m, with its direction varying based on the mode type. When grid imbalances occur, $\tau_{m,t}$ is requested from the TSO. Due to the unpredictability of this request, scenarios \tilde{s} are adapted in the model to account for uncertain energy changes in the SoC during balancing services. These scenarios are derived from balancing service market operation data using scenario generation methods discussed in Section IV. eff_r denotes the charge–discharge efficiency of resource r. For FCR, which is a bidirectional bid, participation is possible when equivalent capacity is ensured in both charging and discharging directions. Constraint (15) ensures that the bidirectional capacity is equivalent to the $SoE_{r,t}$ of Constraint (12) and $P_{r,FCR,t}$.

A model for estimating battery degradation is essential, and two primary categories must be considered: calendar life and cycle life. Calendar life is the natural decline in battery capacity over time, primarily influenced by environmental factors. On the other hand, cycle life represents the maximum number of charge and discharge cycles a battery can undergo, determined by its operational strategy. This research aims to devise a strategy to optimize the cycle life of batteries over a period of 24–48 h. Since the scheduling of electric vehicles typically involves time intervals shorter than an hour, only the cycle life is examined, disregarding the effects of calendar life. Considering that electric vehicle scheduling often involves intervals shorter than one hour, the impact of calendar life is disregarded, focusing solely on cycle life. The total degradation cost formula, based on rainflow-counting algorithm (RCA), is derived from the methodologies outlined in [47]. Fig. 5 illustrates the variation in battery cycle life with the depth of discharge (DoD). It is generally observed that operating at high DoD significantly diminishes the maximum cycle life. This relationship is depicted through an optimized curve, formulated by Eq. (16), where the curve's coefficients (β_0 , β_1 , β_2) are contingent on the battery type and manufacturer-provided experimental data. The cost incurred for a battery to complete one cycle at a given DoD is calculated by dividing the battery capital cost by the maximum number of cycles at that DoD. Since DoD equals 1 - SoC, the cost for one cycle of degradation is expressed as a function of SoC, as delineated in Eq. (17). To apply this in scheduling, two assumptions are made: firstly, that discharge and recharge operations uniformly contribute to degradation until reaching the maximum number of cycles for the corresponding DoD; secondly, that each cycle's impact is independent of the previous cycle.

$$N_{cycle} = \beta_0 \cdot DoD^{-\beta_1} \cdot e^{\beta_2(1-DoD)} \quad (16)$$

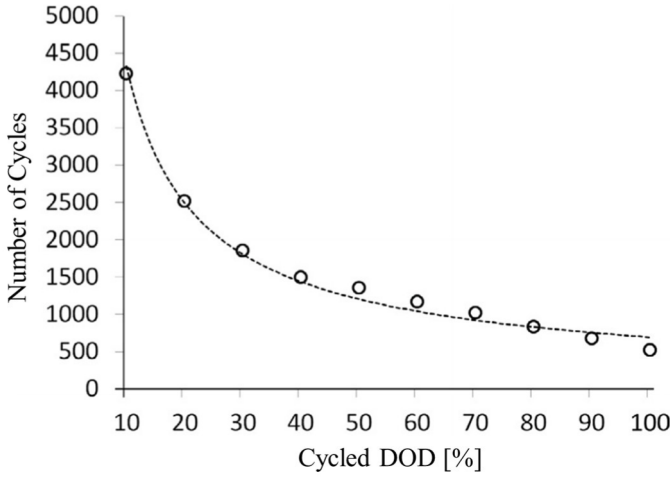


Fig. 5. DoD cycled lithium-ion battery cycle life evaluation.

$$\delta(SoC) = \frac{C_{Batt} \cdot Q_r}{N_{cycle}} \quad (17)$$

$$SoC_{r,t}^{aux}[\bar{s}] = SoC_{r,t-1}[\bar{s}] - \left\{ \sum_{\mathcal{J}} \left(\frac{P_{r,aFRRp,t}}{Q_r} \cdot \tau[\bar{s}]_{aFRRp,t} \right) \cdot eff_r \right\} \quad (18)$$

$$b_{r,t}[\bar{s}] = \delta(SoC_{r,t}^{aux}[\bar{s}]) - \delta(SoC_{r,t-1}[\bar{s}]) \quad (19)$$

When solely real SoCs are employed to represent the total degradation cost based on RCA, the inclusion of non-discrete conditional judgment is necessitated to determine the battery's charging or discharging mode and to calculate the cumulative energy change before mode transition. However, most commercial optimization solvers usually demand linear or quadratic functions for robust solutions. Alternatively, some solvers can address NLP problems with differentiable functions by computing gradient and Hessian matrices. Heuristic algorithms, such as genetic algorithms and PSO, can manage non-differentiable formulations by evaluating the cost of performance degradation from the SoC profile of a particular solution. Nonetheless, these algorithms are computationally intensive and often struggle with handling equality and inequality constraints and adjusting search parameters. To circumvent these challenges, an auxiliary SoC is introduced as indicated in Eq. (18) [47]. The auxiliary SoC is derived from the preceding real SoC, incorporating only the discharge power term. Its purpose is to simplify the expression of the RCA-based battery degradation cost in a mathematically straightforward form, albeit lacking physical interpretability. Thus, the degradation cost function for optimal scheduling, employing both SoC and the auxiliary SoC, is defined in Eq. (19). Although the formulated degradation cost (19) is NLP, owing to the non-convex nature of the optimization problem, it can be seamlessly integrated into MILP by segmenting the SoC of δ into various parts and linearizing them, as depicted in Eq. (20). The superscript seg indicates the segment index, N^{seg} represents the total number of segments, X_t^{seg} is the binary indicator of the segment, m^{seg} denotes the segment slope, and α is the segment gap length. The constraints for this piecewise linearization are outlined as follows:

$$\delta \approx \sum_{seg} [X_t^{seg} \cdot C_E \{ SoC_r^{min} + (seg - 1) \cdot \alpha \} + m^{seg} \cdot SoC_t^{seg}] \quad (20)$$

where

$$m^{seg} = \{ \delta(SoC_r^{min} + \alpha \cdot seg) - \delta(SoC_r^{min} + \alpha \cdot (seg - 1)) \} / \alpha \quad (21)$$

$$\alpha = (SoE_r^{max} - SoE_r^{min}) / N^{seg} \quad (22)$$

Constraint (23) mandates that the SoC, determined by the sum of the segments, must match the SoC calculated using the output power. Constraint (24) ensures that the segmented SoC is confined to the interval length as indicated by the indicator. Lastly, Constraint (25) stipulates that only one segment can be selected for each time step.

$$SoC_r^{min} + \sum_{seg} \{ SoC_t^{seg} + (seg - 1) \cdot \alpha \cdot X_t^{seg} \} = SoC_{r,t}[\bar{s}] \quad (23)$$

$$0 \leq SoC_t^{seg} \leq \alpha \cdot X_t^{seg} \quad (24)$$

$$\sum_{seg} X_t^{seg} = 1 \quad (25)$$

The balancing service market operates with a consecutive 4 h bidding standard, which is termed as bidding product ψ . In the model, consecutive 4 h bidding pools are configured with the same capacity bid, drawing from various combinations in the 1 h resource pool. The most straightforward application binds the sum of the bidding capacity of each 4 h unit in a product with an equality constraint. To simplify the problem, consecutive 4 h bidding is formulated in Constraints (26) and (27). The maximum feasible value of $Bid_{m,\psi}$ is determined by the sum of the bidding capacities of each resource, $P_{r,m,t}^{bid}$, for each time t corresponding to the bidding product ψ . The quotient and modulo operators, abbreviated as *div* and *mod*, are used to achieve this, returning the quotient and remainder after dividing two numbers.

$$Bid_{m,\psi} \leq \Pi_{m,\psi}^{bid}, \forall \psi \in \Psi \quad (26)$$

$$\begin{aligned} \Pi_{m,\psi}^{bid} &\in \left\{ \sum_{\mathbb{R}} P_{r,m,t}^{bid}, \sum_{\mathbb{R}} P_{r,m,t+1}^{bid}, \sum_{\mathbb{R}} P_{r,m,t+2}^{bid}, \sum_{\mathbb{R}} P_{r,m,t+3}^{bid} \right\}, \forall t \bmod 4 \\ &= 0, \forall t \bmod 4 = \psi \end{aligned} \quad (27)$$

In this framework, heavy emphasis is placed on strategic rescheduling to guarantee that accepted bids are fulfilled. The moment when bids are opened daily, t_{open} , serves as a benchmark. Emphasizing the periods leading up to this significant point, a set Ψ' is introduced, defined as: $\Psi' = \{\psi | \psi \leq t_{open}\}$. The model not only establishes the 4 h bidding standard but also integrates backup capacities to reinforce the reliability of the accepted bids. The backup capacities for each 4 h bidding product ψ are outlined in Constraint (28). These capacities, denoted as $\Pi_{m,\psi}^{backup}$, are formulated from various combinations in the 1 h resource pool.

$$\begin{aligned} \Pi_{m,\psi}^{backup} &\in \left\{ \sum_{\mathbb{R}} P_{r,m,t}^{backup}, \sum_{\mathbb{R}} P_{r,m,t+1}^{backup}, \sum_{\mathbb{R}} P_{r,m,t+2}^{backup}, \sum_{\mathbb{R}} P_{r,m,t+3}^{backup} \right\}, \forall t \bmod 4 \\ &= 0, \forall t \bmod 4 = \psi \end{aligned} \quad (28)$$

Subsequently, in Constraint (29), it is ensured that the accepted bid, denoted as $d_{m,\psi}^{ACPT}$, does not exceed the combined sum of the bidding and backup capacities for each product ψ within the set Ψ' .

$$d_{m,\psi}^{ACPT} \leq \Pi_{m,\psi}^{bid} + \Pi_{m,\psi}^{backup}, \forall \psi \in \Psi' = \{\psi | \psi \leq t_{open}\} \quad (29)$$

In Constraint (30), the accepted capacity $ACPT_{m,\psi}$ for each product ψ is constrained by its corresponding accepted bid.

$$ACPT_{m,\psi} \leq Bid_{m,\psi}^{ACPT}, \forall \psi \in \Psi' \quad (30)$$

Through these constraints, the reliability of accepted bids is ensured, and the importance of rescheduling resources to fulfill bid obligations is emphasized, illustrating its pivotal role in the operational strategy.

The TSO uses the log data from a smart meter connected to resources to ensure accurate reserve procurement. This verification process is crucial, particularly when a resource initiates services for the pool, as the procurement is determined based on the CBL. The CBL represents the average power consumed during the 10 min before resource allocation to a pool (Fig. 6). However, every time a resource shifts its allocation

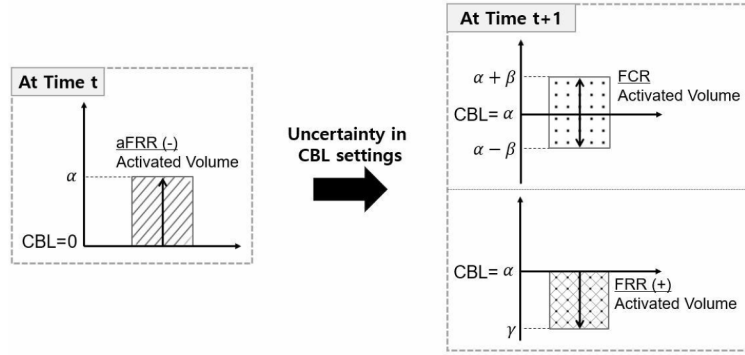


Fig. 6. Uncertainty in the CBL setting due to a replacement in the pool allocation.

between pools, its CBL can be influenced by the procurement from the previous pool, with the exception of the DCM pool. To mitigate the uncertainty associated with CBL, the following rule is introduced: when transitioning between allocated pools, a resource remains idle for a single time slot, as described in (31).

$$\text{IF } UC_{r,m,t-1} == 1, \quad UC_{r,\mathcal{M},Cm,t} = 0 \quad (31)$$

Constraint (31), being a nonconvex set in the form of a conditional statement, was formulated to overcome the uncertainty of the CBL setting. However, it cannot be applied to the model designed using MILP. To address this limitation, constraint (31) was linearized, as shown in Constraint (32).

$$\begin{aligned} \{UC_{r,m,t+1} - UC_{r,m,t}\} + \{UC_{r,m^*,t} - UC_{r,m^*,t+1}\} &\leq 1, \quad \forall m^* \in [m \notin \mathcal{M}], \quad \forall m \\ &\in \{FCR, aFRR\} \end{aligned} \quad (32)$$

Using Constraint (32), the simultaneous commencement of mode m^* 's service and termination of mode \mathcal{M} (excluding m)'s service at time $t+1$ is prevented.

$$\sum_{\mathbb{R}Cback-up} P_{r,m,t}^{bid} \leq \sum_{\mathbb{R}Cbid} P_{r,m,t}^{back-up} \cdot rate^{backup} \quad (33)$$

$$\sum_{\mathbb{R}Cback-up} P_{r,m,t}^{bid} \geq \sum_{\mathbb{R}Cbid} P_{r,m,t}^{back-up} \cdot rate^{backup}$$

Unexpected EV behavior or uncertainties in the volume activated by the balancing service influence aggregator procurement. Two general strategies are typically used to address this shortcoming: 1) bidding with a margin and 2) using an ESS as a backup. In the proposed framework, the ESS was used as a backup and its capacity was dynamically determined based on the bidding pool capacity using Constraint (33). $P_{r,m,t}^{back-up}$ represents the backup capacity for market pools and the charging power for the DCM pool of the r th resource at time slot t in mode m . $rate^{backup}$ denotes the retention rate of the backup resource capacity. The effectiveness and economic viability of capacity retention rate are explored in Section IV.

4. Case study

The optimality and robustness of the proposed model were analyzed based on a) the optimality of revenue maximization and the influence of the uncertainty avoidance condition of the CBL setting, b) robustness against various scenarios and scenario generation method, and c) efficiency and economic feasibility of ESSs based on the capacity retention rate. The Gurobi optimizer, a high-performance solver for mathematical programming, was employed to address the problem formulated as the MILP model. The computations were executed on a system powered by an Intel Core i5-6600 processor with 16 GB of memory and a clock speed of 3.30 GHz. Algorithmic implementation and data processing were

performed using Python programming language.

4.1. Validating optimality and CBL setting uncertainty

Herein, the CBL uncertainty-setting avoidance constraint in the model formulation is validated, and the optimality of the profit maximization and pool allocation of the model is rigorously evaluated. The model is further evaluated using the convergence patterns of an advanced model, and the performance of the model for different EVs and its associated computational efficiency are discussed. Simulation was performed using the 2021–2022 operational data containing the price and volume activated by balancing services [48].

Fig. 7 and Table 3 show the anticipated net revenue when providing the balancing service in 1-MW capacities per bidding product and market on January 29, 2021. The FCR is characterized by only the capacity bid and remains stable within a single product. In contrast, aFRR-p and aFRR-n reserves incorporate energy bids, leading to profit fluctuations based on the volume activated. Except for products 2, 4, and 5, expected net revenues were similar for the remaining binding products. The capacity bid level for products 2, 4, and 5 was similar to that for the other products; however, owing to significant volume activation in the product time zone, a substantial portion of the revenue was obtained from the energy bid. Fig. 8 illustrates the EV configurations employed within the simulation study. In the upper part of Fig. 8, the SoC scenarios for each EV are shown, with black circles representing the forecasted initial SoC and blue triangles denoting the target SoC. The SoC values are determined based on a uniform distribution ranging from 30 % to 80 %. The lower part of the figure illustrates the connection times for the EVs, marked in green, which are the result of a stochastic process modeled by a Markov chain and the Monte Carlo behavior model [49].

Energy market bidding strategies have been extensively studied [6, 37]. However, most studies have overlooked critical factors such as the uniform product sizing regional market and CBL when developing bidding strategies. Ignoring the uniform product sizing regional market could result in strategies that are misaligned with market norms, thereby creating discrepancies in real-time procurement processes. Furthermore, neglecting the CBL might result in an inability to accurately predict and manage consumption variations, potentially undermining the reliability and effectiveness of the bidding strategy. As shown in Table 2, Pandžić et al. [39] ignored both the aforementioned factors and Pavic et al. [7] overlooked the CBL, resulting in bidding strategies that are theoretically flawed and practically unviable, thereby significantly disrupting real-time procurement scenarios. The oversight is rectified by proposing a method that fully integrates these factors into bidding strategy modeling. The resulting strategies are theoretically robust and practically resilient and can navigate the complexities of real-time procurement environments with enhanced reliability and effectiveness.

Fig. 9 shows the comparative analysis of bid capacity and revenue, highlighting the consistent sizing maintained across each bid product. This consistency is ascribed to the model design, which employs various

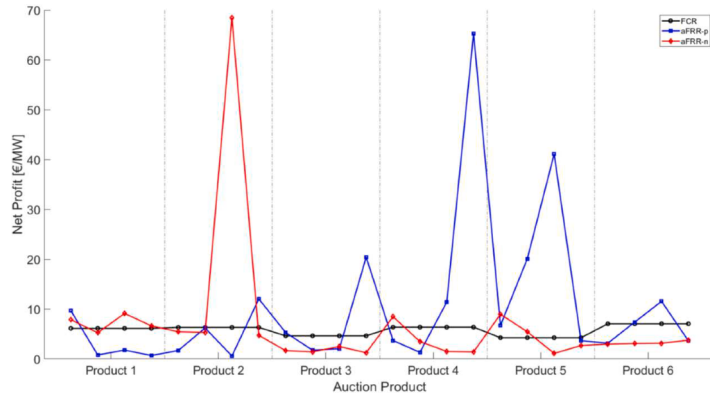


Fig. 7. Daily net revenue by market (January 29, 2021).

Table 3

Net revenue by product (January 29, 2021).

Service Product	FCR	aFRR-p	aFRR-n
1	24.48	12.91	28.83
2	25.24	20.47	83.93
3	18.52	29.47	6.77
4	25.44	81.68	14.84
5	17	71.53	18.16
6	28.16	25.69	12.94

combinations of 1 h resource pools to ensure that the consecutive 4 h bid pools comprise bids with identical capacities. In Fig. 9, the left and right y-axes denote the bid capacity of EVs per hour and the anticipated revenue from these bids, respectively. The dark gray bar graph indicates the bid capacity reported by Pandžić et al. [39], who ignored both the aforementioned factors, and the red line graph illustrates the projected revenue for that bid. The medium-dark gray bar graph shows the bidding capacity presented by Pavic et al. [7], a distinctive study that considers the uniform product sizing regional market and not the CBL, and the green line graph shows the projected revenue for that bid. The lightest gray bar graph presents the outcomes of the proposed method that considers both the factors, and the blue line graph shows the anticipated revenue for those bids. The models proposed by Pandžić

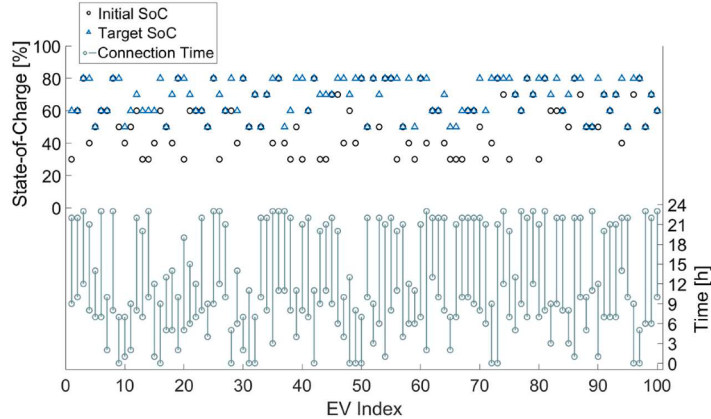


Fig. 8. EV configuration for simulation.

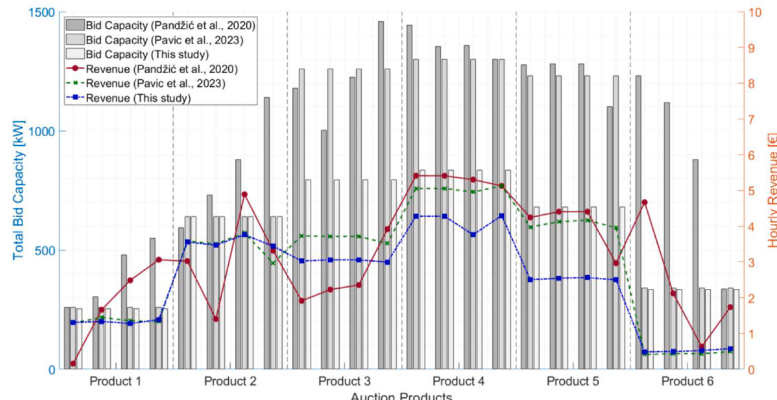


Fig. 9. Comparative analysis of the bid capacity and projected revenue across bidding strategies.

et al. [39] and Pavic et al. [7] are not restricted by variation in pool allocation and consistently opt for the most lucrative pool in each time slot, indicating a pursuit of maximum revenue under the stipulated conditions. Compared with Pavic et al. [7], a more dynamic bidding capacity was proposed by Pandžić et al. [39] as this capacity did not have to maintain uniform sizing within the auction product. The expected revenues for the models proposed by Pandžić et al. [39], Pavic et al. [7], and the current proposed method are 76.83, 72.17, and 60.48 euros, respectively.

However, these projected revenues were calculated based on online evaluations conducted by each model without considering specific rules, and therefore, are not entirely accurate or representative of the expected revenues for genuine auction products. In Germany, auctioned products require a uniform capacity bid spanning 4 h intervals for each market. Fig. 10 shows the proportion of each market in the total bidding capacity per hour, as derived from Fig. 9. The light gray, medium light gray, and dark gray bars denote the share of bidding capacity for FCR, aFRR-p, and aFRR-n, respectively. For auction product 1 [39], aFRR-p bids in the initial time slot and FCR and aFRR-n bid in the subsequent time slots. In this instance, no capacity can be bid for product 1 as uniform bidding for 4 h time slots is unfeasible. This is true for the remaining products; for products 3 and 4, only the minimum bid quantity of FCR constitutes a valid bid capacity. Conversely, a uniform bidding capacity per market across all products is featured by the model suggested by Pavic et al. [7] and the current proposed method.

Nevertheless, there is a significant issue with the bid capacity calculations in relation to the CBL in the study by Pavic et al. [7]. Fig. 11 shows the results of a comprehensive analysis performed to determine the validity of the bid capacity due to the CBL. In this figure, the decisions made by EVs over time are represented by blue circles, progressing from top to bottom. These decisions include idle (no action) participation in the FCR, aFRR-p, and aFRR-n markets and DCM implementation, which facilitates the adjustment of the SoC to the desired levels during operational hours. Fig. 11 shows an instance wherein the EV is connected midway through product 3 and disconnected at the end of product 5, with initial and target SoCs of 40 % and 70 %, respectively. Labels (A), (B), and (C) denote the outcomes from the studies of Pandžić et al. [39], Pavic et al. [7], and the proposed method, respectively. To achieve the charging target, a compulsory 1 h time slot is reserved for the DCM pool allocation, whereas the remainder of the time is used for unrestricted allocation.

The potential for unexpectedly large activation volumes in markets such as aFRR (Fig. 7) is frequently overlooked despite their significant repercussions, particularly at the critical junctures of market transitions. Notably, considerable activation volumes are demonstrated in products 3-(4), 4-(4), and 5-(3) within the aFRR-p sector. Moreover, a 100 % equivalence is attained when the DCM facilitates optimal SoC adjustments for EVs, as analyzed from an activation volume perspective. During market transitions, the CBL becomes significant, where the

default output for the ensuing market response is determined by the DCM and influential factors such as FCR and aFRR. These factors are gauged based on the average output recorded in the last 10 min and play a pivotal role in CBL calculation. The CBL is set to a nonzero value when the DCM, FCR, and aFRR fluctuate during market transitions. This strategy may induce abrupt and unpredictable alterations in the SoC of EVs or ESSs, hampering subsequent market participation. This complex dynamic ensures grid stability but requires skillful management to prevent potential disruptions in procurement processes and ensure seamless transition and operational efficiency.

From this perspective, Pandžić et al. [39] frequently switched markets in nearly every time slot from products 3 to 5, escalating the unpredictability of SoC changes with each time slot. Notably, after the DCM is implemented in product 4-(3), the CBL in product 4-(4) is determined by the charge facilitated by the DCM, which compromises procurement reliability. Conversely, the approach adopted by Pavic et al. [7] is characterized by a less frequent selection of the FCR market compared to the strategy employed by Pandžić et al. [39], particularly opting for the FCR market in product 4-(2) after implementing the DCM in product 4-(1). However, this strategy fails to guarantee procurement reliability, as observed in Pandžić et al.'s approach. In contrast, the proposed method follows a flexible schedule that is unaffected by fluctuations in the activation volume. This strategy is marked by intervals between bids and idle periods during market transitions and results in a reduced bidding capacity (Fig. 9). However, our goal is to establish a robust schedule that minimizes uncertainties and fluctuations linked to CBL adjustments, despite a decrease in bidding volume, to ensure a stable and reliable operational framework.

Fig. 12 shows the discrepancy between the anticipated departure SoC and target SoC for EVs procured using the proposed method. A maximum energy surplus of 2.5 % was observed, indicating that the actual SoC was nearly equivalent to the target SoC for all EVs. Fig. 13 shows the convergence patterns of the advanced model, reflecting the variation in the number of EVs from 2021 to 2022. An examination of 500–1500 EVs was conducted. To ensure precision in simulations, a 1 % tolerance threshold was established and a computational time constraint of 600 s was imposed. The predictive control of the model was executed at a 1 h resolution. Fig. 13(a) shows the optimality gap distribution from the simulations of the advanced model, where the abscissa (x-axis) and ordinate (y-axis) denote the optimality gap and probability distribution, respectively. The observed data revealed that approximately 90 % of the scenarios had a gap not exceeding 1 %, peaking at 3.5 %. For EV scheduling and optimization in energy and ancillary service markets, an optimality gap tolerance between 1 % and 5 % is deemed acceptable because such gaps infrequently lead to significant performance degradations [50]. Fig. 13(b) shows that the computational time increases with as the number of EVs increases. The annual mean computational time for each EV is represented by the plotted lines, with the shaded regions indicating 95 % confidence interval. For 1000 EVs, solutions

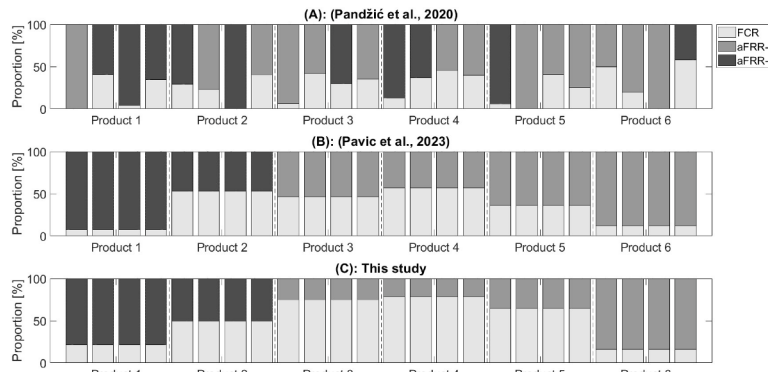


Fig. 10. Market share analysis of bidding capacity per hour with a focus on uniformity across auction products.

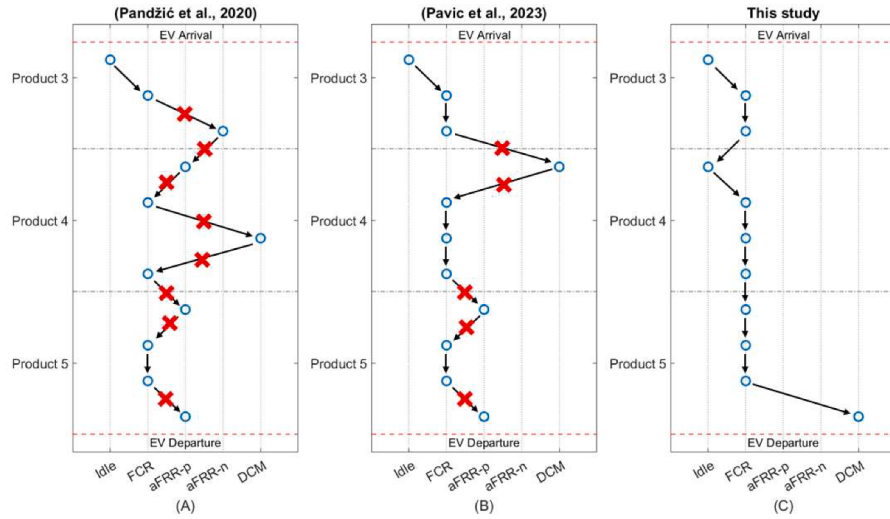


Fig. 11. EV decision progression over time: a detailed analysis of SoC adjustments and market participation strategies.

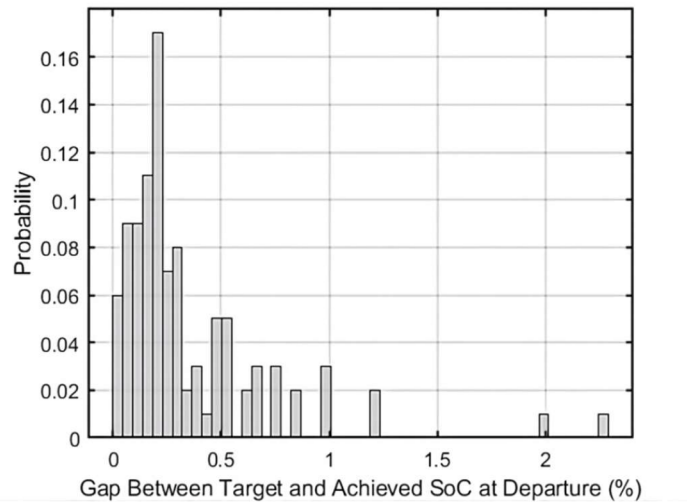


Fig. 12. Gap analysis between estimated departure and target SoC in EVs using the proposed method.

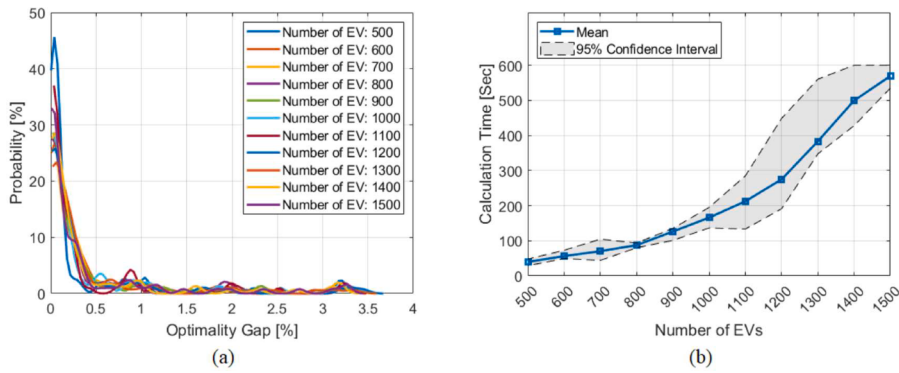


Fig. 13. Analysis of (a) optimality gap distribution and (b) computational time in the proposed model.

were achieved within 180 s. The computational time reached the 600 s limit for a large number of EVs. However, as highlighted in Fig. 13(a), even when computations were halted due to the set stopping parameter, the resulting scheduling outcome exhibited an optimality gap between 1 % and 3.5 %.

The evaluation of the proposed method for including degradation in the bidding strategy is undertaken by applying it to three distinct batteries—B1, B2, and B3. The coefficients for their battery curves, which are critical to this analysis, are detailed in Table 4 [47]. The outcomes of this application are then conveyed in Fig. 14; specifically,

part (a) illustrates the bidding results for battery B1, where the proposed method that incorporates battery degradation is contrasted with the model that excludes such considerations by omitting Eqs. (16)–(25). In Fig. 14(b), the expected revenue and degradation costs associated with each method are then depicted, showing a more conservative bidding approach has been adopted with the proposed method in comparison to the model without degradation. This is evidenced by the reduced bidding on specific products such as 3 and 5. Despite the more conservative bidding, it is shown that the expected revenue remains relatively unaffected, sustaining levels similar to those of the non-degradation model, while a reduction in degradation costs is also noted. Expanding upon these findings, Table 5 presents a comparison of the revenues and degradation costs for the three batteries under both the model that excludes degradation and the proposed method that includes it. It is observed that although the non-degradation model is associated with higher immediate revenues, the proposed method, when factoring in degradation costs, results in higher total revenues for all batteries, thereby substantiating the proposed method's efficacy.

Figs. 15 and 16 show the applicability of the proposed method in the EU; the left y-axis denotes the hourly bidding capacity of EVs, similar to Fig. 9, and the right y-axis denotes the net revenue for each market when a bid of 1 MW is placed, similar to Fig. 7. Fig. 15 shows the bidding results of the proposed method for Finland based on previously reported data [51]. The bar graphs in blue, red, and yellow represent the bidding capacities of FCR, aFRR-p, and aFRR-n, respectively. Correspondingly, the line graphs shown in the same colors illustrate the temporal variation in the net revenue of FCR, aFRR-p, and aFRR-n. The net revenue graph fluctuates hourly, a phenomenon attributed to the energy compensation characteristic of Finland's FCR. The aFRR market is generally more lucrative and offers higher capacity compensation compared to the FCR. Moreover, a slight edge in profitability was noted for aFRR-p over aFRR-n, with a predominant focus on aFRR-p bidding. Significant bidding was also observed in the FCR market, a trend attributed to the smaller SoC fluctuations induced by the two-way response of the FCR, which maintained the SoC at a reasonable level. Fig. 16 shows the bidding results for France based on the previously reported data [52]. The blue and red graphs represent the FCR and aFRR bidding capacities of the proposed method, respectively, along with their corresponding hourly net revenues. Notably, the aFRR market in France is characterized by symmetric bidding, eliminating the need for separate aFRR-p and aFRR-n markets. This market, similar to Finland, generally offers larger capacity rewards compared to FCR, making it more profitable. However, the bidding capacity for FCR was smaller than that for aFRR owing to the bidirectional nature of aFRR, which mitigates the strong unidirectional SoC fluctuations and yields higher revenues than FCR.

In conclusion, a marked distinction is observed between the proposed method and previous studies, primarily because it is adept at handling the critical gaps in the current literature. Furthermore, the proposed method is scalable across the EU market landscape and is a vital tool for real-world revenue-related applications. Notably, it can increase profitability, which highlights its practicality and pivotal role in the advancement of energy market bidding strategies.

4.2. Scenario-based robustness verification

The robustness of the proposed method was evaluated by generating various scenarios from the operational data related to the volume

Table 4
Coefficients of battery degradation curves [47].

Battery	β_0	β_1	β_2
B1	4901	1.98	0.16
B2	3832	0.68	1.64
B3	3141	1.6	8.7×10^{-5}

activated by the balancing service. The scenario generation framework proceeded as follows:

- Operational data were scrutinized and classified based on the identified characteristics.
- Scenarios were generated by applying the Monte Carlo scenario generation method to the classified data.
- The robustness of the model was then evaluated under the generated scenarios.

Operational data from 2021 to 2022 were used for scenario generation, and 1000 scenarios were assessed. The aFRR-p and aFRR-n were initially analyzed. Given the nature of balancing services, which activate during grid imbalances, no significant patterns in volume activation occurrences were determined. However, as imbalances arise from power demand fluctuations, the frequency and intensity of occurrences were segmented and examined based on times that best depicted demand characteristics (Figs. 17 and 18). The x- and y-axes represent the time and volume-activated intensity [%], respectively, whereas the z-axis indicates occurrence frequency. In the aFRR, procurement direction was bifurcated into positive and negative directions. Notably, high-intensity volume activations exhibited hourly occurrence trends. Positive procurement predominantly manifested during mornings and evenings, aligning with sudden demand surges that caused power generation deficits; negative procurement showed an inverse pattern. Low activated volumes displayed uniform distribution without pronounced features. Fig. 19 shows a histogram of volume activation by time. Approximately 95 % of the volume-activated ratio is lower than 7 %, and the standard deviations differ over time but maintain the same shape.

The operational data do not include the FCR-activated volume, which was estimated from the frequency data for Germany [53]. Fig. 20 presents a histogram of the 2021 frequency data for Germany, which closely aligns with a normal distribution. The probabilities of grid imbalances occurring at 0.0360 and 0.0474 Hz are 95 % and 99 %, respectively. Δf^{param} provided by the TSO was assumed to be 0.2–1 Hz. Fig. 21 shows the corresponding droop curve for Δf^{param} .

Fig. 22 shows the outcomes of the verification for scenarios generated using the Monte Carlo scenario generation method. This figure represents the ratio of failure scenarios based on energy fluctuations from the volume-activated ratio of aFRR and Δf^{param} . A scenario is considered a failure if the SoC of an EV surpasses its capacity range. These results were derived by adjusting the standard deviations of the hourly histogram distribution of aFRR by considering potential variances in the volume-activated ratio. When Δf^{param} values were 0.5–1 Hz, <1 % failure scenarios were noted. When Δf^{param} values were 0.2–0.3 Hz, which are associated with significant volume activations, <5 % failure scenarios were noted. These findings confirm the reliability of the proposed model in relation to the volume activated by the balancing service.

For the purpose of elucidating the model's robustness, Fig. 23 depicts the random behaviors of EVs that follow a normal distribution. Deviations from anticipated scenarios, within an error margin of 2σ ranging from 5 % to 30 %, are detailed, as explicated by [54]. The upper part of the figure shows the SoC scenarios for each EV, where the black circles represent the original forecasted initial SoC, the red 'x' marks indicate the actual initial SoC, and the blue triangles denote the target SoC. The lower part of the figure presents the charging times, with green marks for the estimated times and red diamonds for the observed variations, demonstrating the instances of discrepancy from the original estimates. Taking EV2 as a case in point, the figure illustrates that its projected initial SoC is at 60 %, while the actual initial SoC is recorded at 57.68 %, and the target SoC is aimed at 60 %. The intended connection time for charging was scheduled from 10 am to 10 pm. However, the actual connection period as shown was from 11 am to 9 pm, with the plug-in time commencing one hour later and finishing an hour earlier than planned.

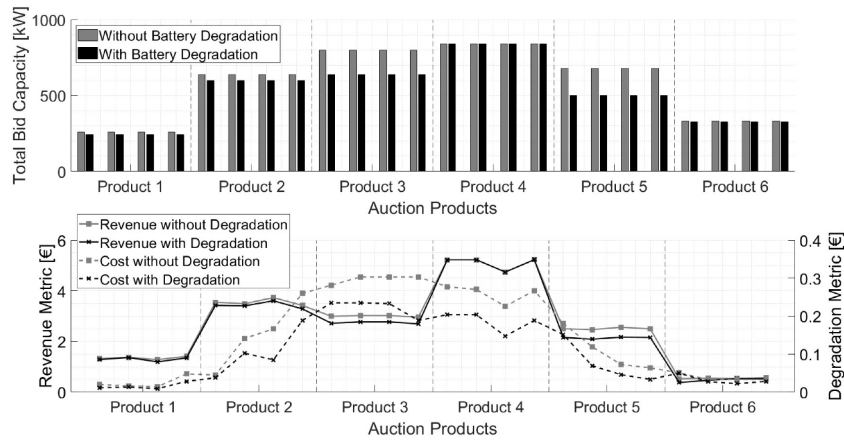


Fig. 14. Comparison of bidding results and expected revenue for battery B1: without degradation vs. proposed degradation method.

Table 5

Revenue and degradation cost comparison for batteries B1, B2, and B3.

Model	Revenue [€]			Battery degradation cost [€]			Total revenue [€]		
	B1	B2	B3	B1	B2	B3	B1	B2	B3
W/O degradation	64.175	64.175	64.175	4.926	5.099	5.035	59.249	59.076	59.14
RCA	62.33	62.154	62.216	2.335	2.742	2.891	59.995	59.412	59.325

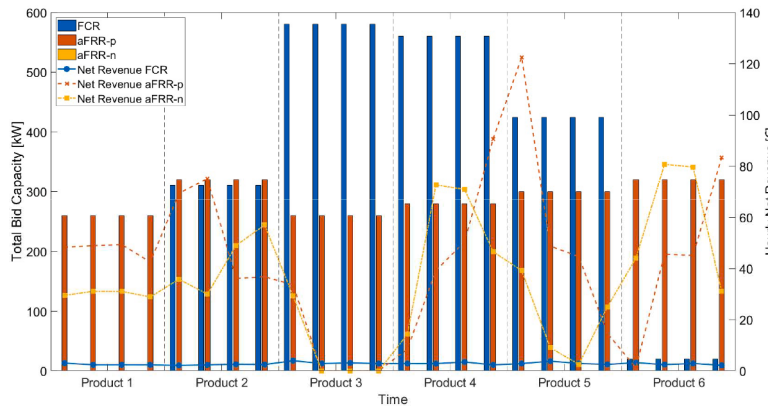


Fig. 15. Comparative analysis of bidding capacities and net revenues in Finland's balancing market (January 29, 2021).

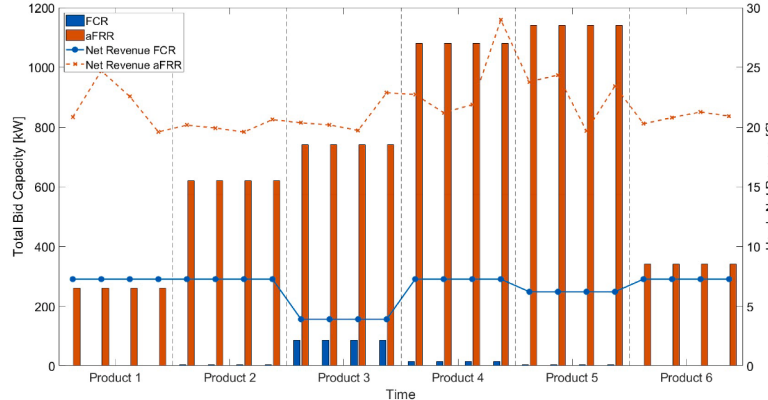


Fig. 16. Comparative analysis of bidding capacities and net revenues in France's balancing market (January 29, 2021).

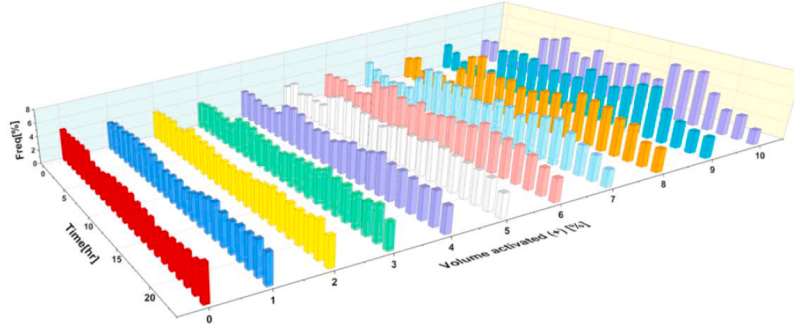


Fig. 17. aFRR-p volume-activated ratio distribution by time.

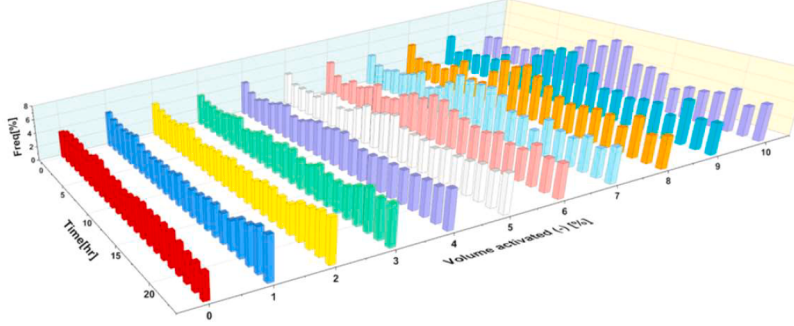


Fig. 18. aFRR-n volume-activated ratio distribution by time.

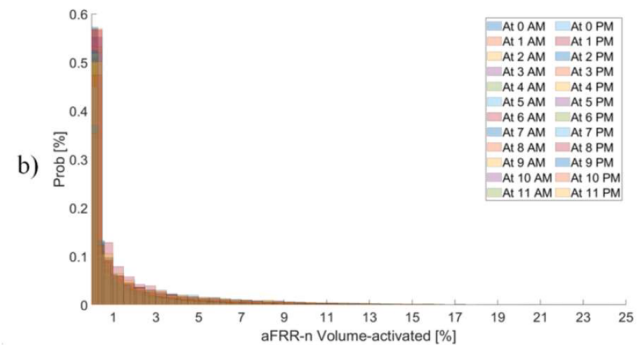
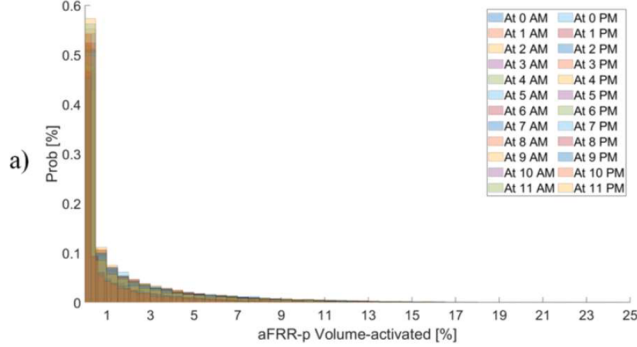


Fig. 19. Histogram of a) aFRR-p and b) aFRR-n volume-activated ratio by time (2021–2022).

Fig. 24 presents the scheduling outcomes for resource allocation rescheduling, designed to maintain the accepted capacity each hour, in the face of variations in the standard deviation σ and a frequency deviation parameter Δf^{param} of 0.2 Hz. The black line graph across the figure represents the accepted capacity to be procured for each hour.

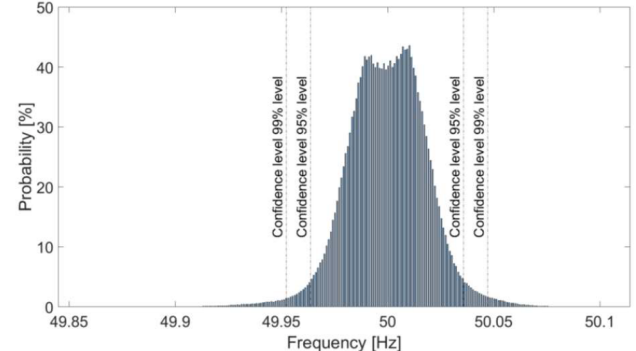


Fig. 20. Histogram of grid frequency, Germany, 2021.

Below this line, the figure features six stacked bar graphs per time slot, indicating the procurement achieved: dark gray bars show the capacity procured by EVs, and light gray bars represent the capacity from backup ESS, with the total capacity measured in kW. These bars are arranged to reflect the total procurement capacity for EVs and backup ESS as the 2σ increases in increments of 5 % from 5 % to 30 %. This is particularly evident in a yellow-highlighted section to the right of the figure, where the bar graphs for the 24th time slot are enlarged, providing a detailed view of the procurement for each increment of 2σ . The simulation results, which passively map the interaction between Δf^{param} and σ , are compiled into Table 6. This table passively documents the shifting reliance on backup ESS with increasing volatility, depicted by 2σ values that range from 5 % to 30 %, and a Δf^{param} that adjusts between 0.5 Hz and 0.2 Hz. It is indicated that when 2σ is at or below 10 %, EVs can nearly manage procurement on their own. As 2σ exceeds 15 %, an increase in the contribution of backup ESS to procurement is noted, beginning at 1.413 %. The reliance on backup ESS becomes markedly pronounced at a 2σ of 30 %, where up to 12.914 % of the total procurement capacity is attributed to backup ESS at a Δf^{param} of 0.2 Hz,

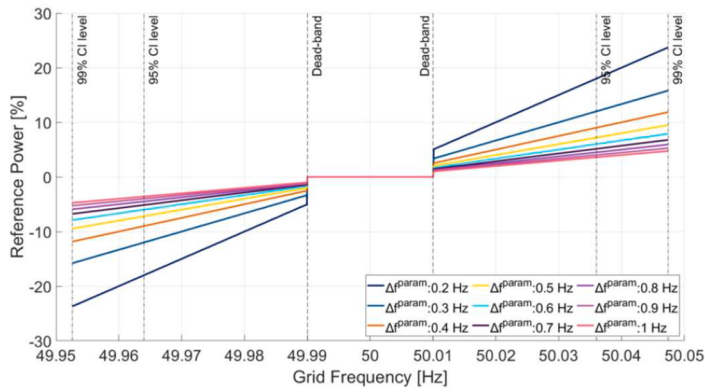
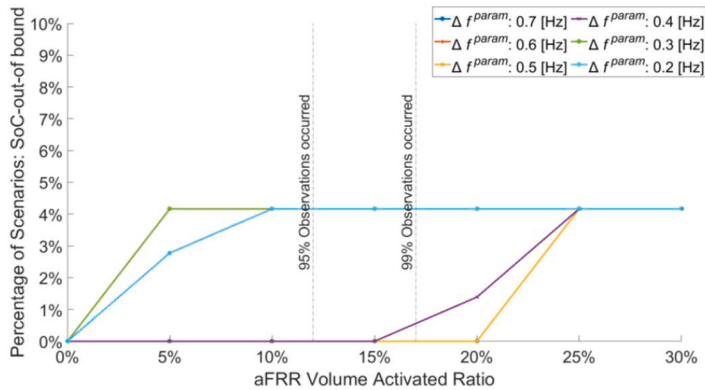
Fig. 21. Droop curve with deadband for Δf^{param} .

Fig. 22. Result of verifying the robustness of the proposed model based on suggested scenario.

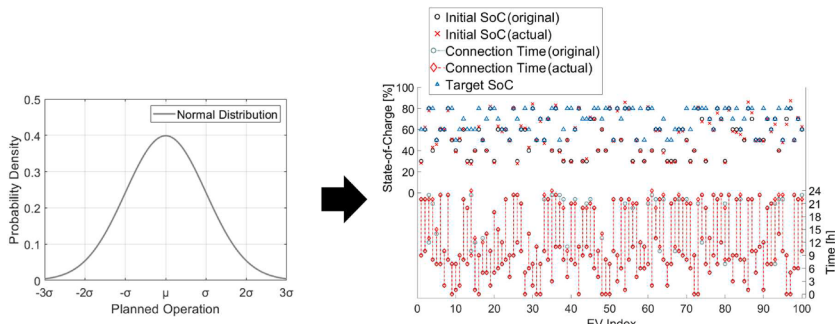
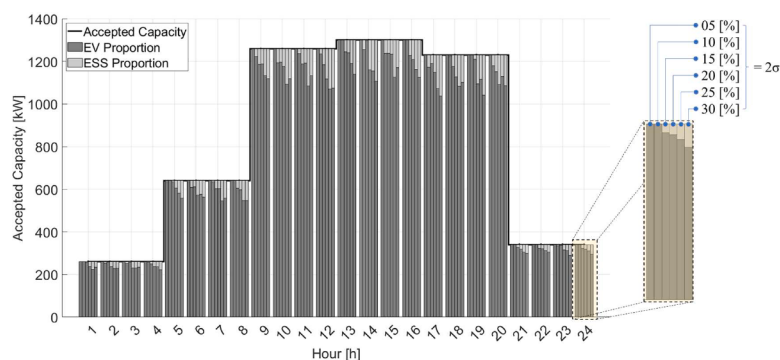
Fig. 23. Actual scenario representation at $2\sigma = 5\%$.Fig. 24. Proportion of EV and ESS procurement capacities across various σ levels under $\Delta f^{param} = 0.2\text{Hz}$.

Table 6

Dependency ratios of backup ESS in procurement across volatility (σ) and frequency deviation scenarios (Δf^{param}).

Δf^{param} 2σ	0.5 Hz	0.4 Hz	0.3 Hz	0.2 Hz
5 %	0	0	0	0
10 %	0	0	0	1.358
15 %	1.413	1.698	2.069	3.082
20 %	2.343	4.367	5.214	7.670
25 %	2.727	6.039	8.272	11.606
30 %	4.897	7.842	10.097	12.914

indicating that the integration of backup ESS into the framework effectively shields the procurement process from the variability in EV behavior.

4.3. Efficiency and economic validation of ESS by capacity retention

The effectiveness and economic feasibility of using an ESS to address procurement failures were investigated. The uncertain behavior of EVs was assessed based on the EV presence rate for each allocated pool; the results provided a guideline for determining the capacity retention rate of the quantitative-backup ESS in the proposed model.

The EV presence rate is defined as the ratio of the actual number of EVs to the anticipated number of connected EVs, which determines the bidding capacity of the allocated pool. A decline in the EV presence rate implies that a single EV must accommodate large SoC fluctuation based on the gateway operator's command. In extreme cases, this could result in procurement failures during the bidding product. In contrast, an EV presence rate exceeding 100 % implies that an additional EV must be used for backup. Figs. 25–28 show the proportion of failure scenarios in relation to the EV presence rate and ESS capacity retention rate. Each graph shows the variation in the Δf^{param} of FCR. As the SoC volatility error increases due to a diminishing EV presence rate, failure scenarios sharply increase, beginning at 5 %, when the presence rate falls below roughly 80 %. A reduction in Δf^{param} increases the SoC fluctuation rate. The subsequent figures display an even steeper increase in the failure scenario rate. As the ESS capacity retention rate increases the coverable capacity, the failure scenario rate declines.

While failure scenarios are identified, determining the optimal storage capacity by considering utility and economic feasibility based on the ESS capacity retention rate is crucial. Table 7 shows the ESS price factors used to compute the maintenance cost in relation to the ESS capacity retention rate. The costs associated with the ESS are considered as outlined below:

$$C^{ESS} = (C^{PCS} + C^{Batt} + C^{BOP}) \cdot \phi + C^{O&M} \quad (34)$$

subject to

$$C^{PCS} = C^{PCSUunit} \cdot P_{r,m,t}^{backup} \quad (35)$$

$$Q^{backup} = \|\sum_{\psi} \{Bid_{m,\psi}\} \cdot rate^{backup}\|_{\infty}, \forall \psi \in \Psi \quad (36)$$

$$C^{Batt} = C^{BattUnit} \cdot \sum_{\psi} \sum_{\mathcal{M}} \{Bid_{m,\psi}\} \cdot rate^{backup} \quad (37)$$

$$C^{BOP} = C^{BOPUnit} \cdot \sum_{\psi} \sum_{\mathcal{M}} \{Bid_{m,\psi}\} \cdot rate^{backup}$$

$$C^{O&M} = C^{O&MUnit} \cdot \sum_{\psi} \sum_{\mathcal{M}} \{Bid_{m,\psi}\} \cdot rate^{backup}$$

$$\phi = \frac{i_r \cdot (1 + i_r)^y}{(1 + i_r)^y - 1} \quad (38)$$

Eqs. (34)–(38) show the formula for calculating the cost of an ESS in four categories: (i) the cost associated with the power conversion system, (ii) cost of the battery, (iii) balance of the plant's cost, and (iv) annual operation and maintenance (O&M) of ESSs. The factor ϕ , representing the weights among the four types of costs, is defined in Eq. (34). The total cost of the power conversion system based on the rated output power of the ESS for backup $P_{r,m,t}^{backup}$ and the unit cost of power electronics is calculated using Eq. (35). The ESS capacity, which is proportional to the maximum value of the sum of all bid pool capacities based on the retention rate, is determined using Eq. (36). Eq. (37) is used to determine the cost of an ESS, the total cost of the balance of the plant, and the capital recovery factor. These costs are derived using the unit cost of the storage devices ($C^{BattUnit}$), unit cost of the balance of the plant (C^{BOP}), and fixed O&M cost ($C^{O&M}$) for the ESS capacity (Q^{backup}). Finally, the capital recovery factor, considering the component's lifetime (y) and annual interest rate (i_r), is computed using Eq. (38).

Fig. 29 shows the reduction in balancing service revenue influenced by the ESS capacity retention rate. To establish an optimal retention rate, the cost and utility of ESS capacity against potential balancing service revenue must be evaluated. If the acquisition and maintenance cost of ESSs surpass the potential revenue from the balancing market, bypassing the ESS investment might be more cost-effective. Instead, bids can be formulated based on the actual presence rate of EVs with an acceptable margin of failure. This model considers the economic rationale of investing in an ESS to mitigate potential failures in the balancing service.

5. Conclusions and future work

This study proposed a comprehensive method to enhance the participation of EVs in the German balancing market. Although the primary focus was on the German market, the proposed method can be applied across various European energy markets. A robust framework was presented, emphasizing the integration of EVs and ESSs into the flexibility market. Primarily, an innovative multimarket bidding strategy was introduced, meticulously designed to increase market

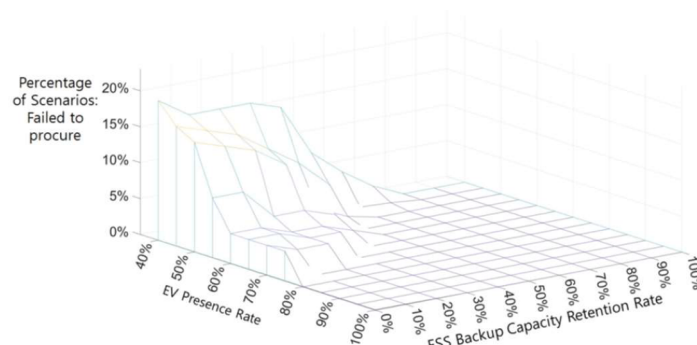


Fig. 25. Failure scenario rate according to the EV presence rate and ESS capacity retention rate, $\Delta f^{param} : 0.5 \text{ Hz}$.

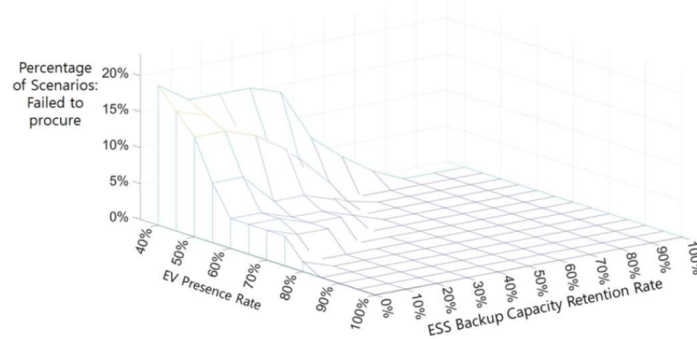


Fig. 26. Failure scenario ratio according to EV presence rate and ESS capacity retention rate, $\Delta f^{param} : 0.4 \text{ Hz}$.

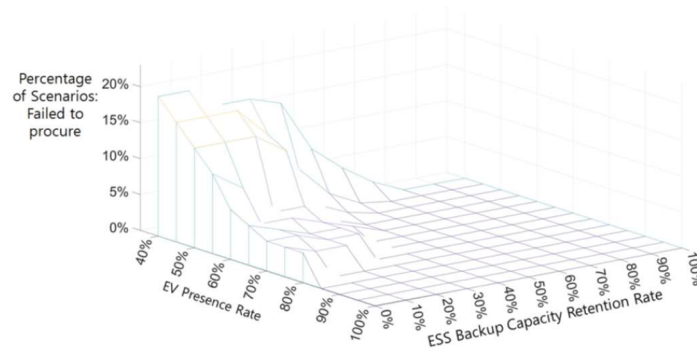


Fig. 27. Failure scenario ratio according to EV presence rate and ESS capacity retention rate, $\Delta f^{param} : 0.3 \text{ Hz}$.

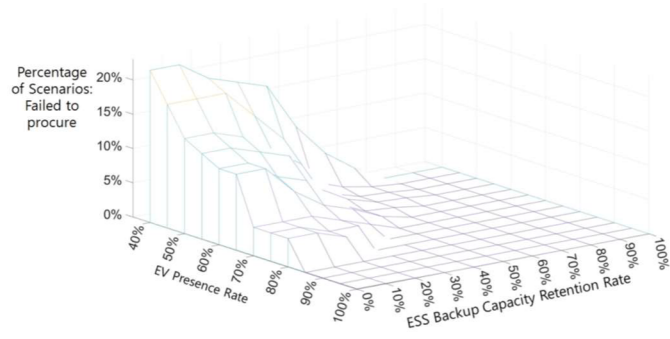


Fig. 28. Failure scenario ratio according to EV presence rate and ESS capacity retention rate, $\Delta f^{param} : 0.2 \text{ Hz}$.

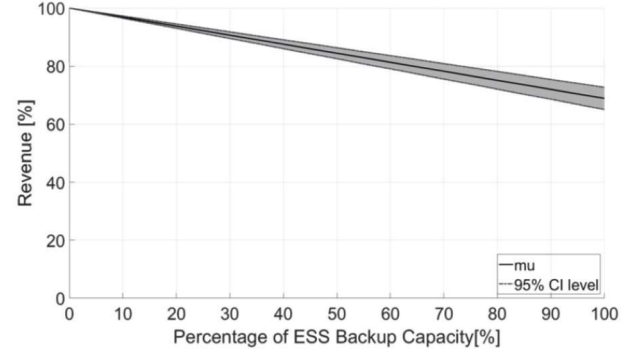


Fig. 29. Balancing services market participation scenario and simulation results.

discussed. Overall, this study will support future research on EV market participation by establishing benchmarks in practicality, innovation, and market depth.

In the modeling for the balancing market conducted by this study, the challenge was presented by the unpredictable arrival and departure times of EVs. This was addressed by integrating periodic resource rebalancing and the inclusion of an ESS as backup, utilizing scenario-based stochastic optimization. While this approach has been effective, it is recognized that it might not capture all real-time behaviors of EVs, suggesting areas for further refinement. Techniques such as neural networks and time series forecasting are to be explored in future efforts, supported by real-time data analytics, to improve the understanding and prediction of stochastic EV behaviors. This enhanced method aims to incorporate uncertainties into the optimization framework more effectively, ensuring optimal decisions by aggregators in the face of EV unpredictability. Additionally, the study acknowledges the challenges brought about by battery degradation, including its nonlinear dynamics

efficiency. The study determined the complexities of market depth by incorporating elements such as uniform product sizing and CBL. By exploring the unpredictable behavior of EVs in depth, insights into potential procurement failures were provided. Further, the study discussed optimization strategies for ESS reserves to ensure high system reliability. The robustness of the proposed model was validated through scenario-based assessments and its potential for practical applications was

and complex physical properties. The influence of procurement activities on battery degradation, particularly regarding market participation, will be a central focus of subsequent research. The objective is to integrate this understanding into the revenue analysis framework, aiming for a comprehensive view of revenue streams while considering the intricacies of battery behavior.

CRediT authorship contribution statement

Mingyu Seo: Conceptualization, Formal analysis, Investigation, Methodology, Software, Visualization, Writing – original draft. **Yuwei Jin:** Project administration, Writing – review & editing. **Musu Kim:** Visualization. **Hyeongyu Son:** Resources. **Sekyung Han:** Supervision, Writing – review & editing.

Declaration of Competing Interest

The authors declare the following financial interests/personal relationships which may be considered as potential competing interests:

Sekyung Han reports financial support was provided by Korea Electrotechnology Research Institute and Korea Institute of Energy Technology Evaluation and Planning.

Data availability

<https://www.smard.de/en>

Acknowledgments

This work was supported by the Human Resources Program in Energy Technology of the Korea Institute of Energy Technology Evaluation and Planning (KETEP) granted financial resource from the Ministry of Trade, Industry & Energy, Republic of Korea (No. 20204010600060). Additionally, this research received support from the Korea Electrotechnology Research Institute (KERI) Primary research program through the National Research Council of Science & Technology (NST) funded by the Ministry of Science and ICT (MSIT) (No. 23A01069).

References

- [1] M.J.B. Kabeyi, O.A. Olanrewaju, Sustainable energy transition for renewable and low carbon grid electricity generation and supply, in: *Frontiers in Energy Research*, 9, Frontiers Media S.A., 2022, <https://doi.org/10.3389/fenrg.2021.743114>.
- [2] X. Luo, J. Wang, J.D. Wojcik, J. Wang, D. Li, M. Dragomescu, Y. Li, S. Miao, Review of voltage and frequency grid code specifications for electrical energy storage applications, *Energies* 11 (5) (2018), <https://doi.org/10.3390/en11051070>. MDPI AG.
- [3] Commission regulation (EU) 2017/ 2195 - of 23 November 2017 - establishing a guideline on electricity balancing. (2017).
- [4] J. Tan, Y. Zhang, Coordinated control strategy of a battery energy storage system to support a wind power plant providing multi-timescale frequency ancillary services, *IEEE Trans. Sustain. Energy* 8 (3) (2017) 1140–1153, <https://doi.org/10.1109/TSTE.2017.2663334>.
- [5] K. Dehghanpour, S. Afsharnia, Electrical demand side contribution to frequency control in power systems: a review on technical aspects, in: *Renewable and Sustainable Energy Reviews*, 41, Elsevier Ltd, 2015, pp. 1267–1276, <https://doi.org/10.1016/j.rser.2014.09.015>.
- [6] P. Hasanpor Divshali, C. Evens, Optimum operation of battery storage system in frequency containment reserves markets, *IEEE Trans. Smart Grid* 11 (6) (2020) 4906–4915, <https://doi.org/10.1109/TSG.2020.2997924>.
- [7] I. Pavic, H. Pandzic, T. Capuder, Electric vehicle aggregator as an automatic reserves provider under uncertain balancing energy procurement, *IEEE Trans. Power Syst.* 38 (1) (2023) 396–410, <https://doi.org/10.1109/TPWRS.2022.3160195>.
- [8] A. Papavasiliou, Y. Smets, G.de M D'aertrycke, Market design considerations for scarcity pricing: a stochastic equilibrium framework, *Energy J.* 42 (5) (2021) 195–220, <https://doi.org/10.5547/01956574.42.5.apa>.
- [9] H. Algarvio, F. Lopes, A. Couto, J. Santana, A. Estanqueiro, Effects of regulating the European internal market on the integration of variable renewable energy, in: *Wiley Interdisciplinary Reviews: Energy and Environment*, 8, John Wiley and Sons Ltd, 2019, <https://doi.org/10.1002/wene.346>.
- [10] Electric vehicles - IEA. (n.d.). Retrieved August 28, 2023, from <https://www.iea.org/energy-system/transport/electric-vehicles>.
- [11] L. Ciabattoni, S. Cardarelli, M. Di Somma, G. Graditi, G. Comodi, A novel open-source simulator of electric vehicles in a demand-side management scenario, *Energies* (6) (2021) 14, <https://doi.org/10.3390/en14061558>.
- [12] M.A. Alotaibi, A.M. Eltamaly, Upgrading conventional power system for accommodating electric vehicle through demand side management and V2G concepts, *Energies* (18) (2022) 15, <https://doi.org/10.3390/en15186541>.
- [13] Y. Zheng, Y. Wang, Q. Yang, Two-phase operation for coordinated charging of electric vehicles in a market environment: from electric vehicle aggregators' perspective, *Renew. Sustain. Energy Rev.* 171 (2023), <https://doi.org/10.1016/j.rser.2022.113006>.
- [14] D. Schwabeneder, C. Corinaldesi, G. Lettner, H. Auer, Business cases of aggregated flexibilities in multiple electricity markets in a European market design, *Energy Convers. Manag.* 230 (2021), <https://doi.org/10.1016/j.enconman.2020.113783>.
- [15] V. Silva, M. López-Botet Zulueta, Y. Wang, P. Fourment, T. Hinchliffe, A. Burtin, C Gatti-Bono, Anticipating some of the challenges and solutions for 60% renewable energy sources in the european electricity system, in: *Springer Proceedings in Mathematics and Statistics* 254, 2018, pp. 169–184, https://doi.org/10.1007/978-3-319-99052-1_9.
- [16] F. Bovera, G. Rancilio, D. Falabretti, M. Merlo, Data-driven evaluation of secondary-and tertiary-reserve needs with high renewables penetration: the Italian case, in: , 2021, p. 14, <https://doi.org/10.3390/en14082157>.
- [17] www.regelleistung.net >general info >what is control energy? (Prequalification). (n.d.). Retrieved August 28, 2023, from <https://www.regelleistung.net/en-us/General-info/What-is-control-energy-Prequalification>.
- [18] Motte Cortés, A., & Eising, M. (2019). Assessment of balancing market designs in the context of European coordination. <https://doi.org/10.1109/EEM.2019.8916481>.
- [19] A. Gonçearuc, N. Sapountzoglou, C. De Cauwer, T. Coosemans, M. Messagie, T. Crispeels, Profitability evaluation of vehicle-to-grid-enabled frequency containment reserve services into the business models of the core participants of electric vehicle charging business ecosystem, *World Electr. Veh. J.* 14 (1) (2023), <https://doi.org/10.3390/wev14010018>.
- [20] N. Brinkel, M. Zijlstra, R. van Bezu, T. van Twijver, I. Lampropoulos, W. van Sark, A comparative analysis of charging strategies for battery electric buses in wholesale electricity and ancillary services markets, *Transp. Res. Part E: Logist. Transp. Res.* 172 (2023), <https://doi.org/10.1016/j.tre.2023.103085>.
- [21] I. Pavic, H. Pandzic, T. Capuder, Day-ahead energy and balancing capacity bidding considering balancing energy market uncertainty, in: *SEST 2022 - 5th International Conference on Smart Energy Systems and Technologies*, 2022, <https://doi.org/10.1109/SEST53650.2022.9898473>.
- [22] W. Vermeer, G.R.C. Mouli, P. Bauer, Optimal sizing and control of a PV-EV-BES charging system including primary frequency control and component degradation, *IEEE Open J. Ind. Electron. Soc.* 3 (2022) 236–251, <https://doi.org/10.1109/OJIES.2022.3161091>.
- [23] J. Villar, R. Bessa, M. Matos, Flexibility products and markets: literature review, in: *Electric Power Systems Research*, 154, Elsevier Ltd, 2018, pp. 329–340, <https://doi.org/10.1016/j.epsr.2017.09.005>.
- [24] M. Bostan, EU electricity policy (IM)balance: a quantitative analysis of policy priorities since 1986, *Int. J. Energy Econ. Policy* 11 (5) (2021) 298–309, <https://doi.org/10.32479/ijep.11461>.
- [25] D. Lazović, Ž. Đurišić, Advanced flexibility support through DSO-coordinated participation of DER aggregators in the balancing market, *Energies* (8) (2023) 16, <https://doi.org/10.3390/en16083440>.
- [26] M. Merten, C. Olk, I. Schoeneberger, D.U. Sauer, Bidding strategy for battery storage systems in the secondary control reserve market, *Appl. Energy* 268 (2020), <https://doi.org/10.1016/j.apenergy.2020.114951>.
- [27] G. Angenendt, M. Merten, S. Zurmühlen, D.U. Sauer, Evaluation of the effects of frequency restoration reserves market participation with photovoltaic battery energy storage systems and power-to-heat coupling, *Appl. Energy* 260 (2020), <https://doi.org/10.1016/j.apenergy.2019.114186>.
- [28] K. Jacqué, L. Koltermann, J. Figgener, S. Zurmühlen, D.U. Sauer, The influence of frequency containment reserve on the operational data and the state of health of the hybrid stationary large-scale storage system, *Energies* (4) (2022) 15, <https://doi.org/10.3390/en15041342>.
- [29] M.T. Muhsin, L.M. Cipciyan, S.S. Sami, Z.A. Obaid, Potential of demand side response aggregation for the stabilization of the grids frequency, *Appl. Energy* 220 (2018) 643–656, <https://doi.org/10.1016/j.apenergy.2018.03.115>.
- [30] K. Poplavskaya, J. Lago, L. de Vries, Effect of market design on strategic bidding behavior: model-based analysis of European electricity balancing markets, *Appl. Energy* 270 (2020), <https://doi.org/10.1016/j.apenergy.2020.115130>.
- [31] What is aFRR (automatic frequency restoration reserve)? (n.d.). Retrieved August 28, 2023, from <https://www.next-kraftwerke.com/knowledge/afr>.
- [32] RTE report on balancing 2020-2021, two years of balancing the French electric system. (n.d.).
- [33] Oyj, F. (n.d.). Unofficial translation terms and conditions for providers of automatic frequency restoration reserves (aFRR).
- [34] System operations. (n.d.). Retrieved August 28, 2023, from https://www.entsoe.eu/network_codes/sys-ops/.
- [35] Frequency ancillary services terms and conditions. (2020).
- [36] M. Barbero, C. Corchero, L. Canals Casals, L. Igualada, F.J. Heredia, Critical evaluation of European balancing markets to enable the participation of demand aggregators, *Appl. Energy* 264 (2020), <https://doi.org/10.1016/j.apenergy.2020.114707>.

- [37] F. Nitsch, M. Deissenroth-Uhrig, C. Schimeczek, V. Bertsch, Economic evaluation of battery storage systems bidding on day-ahead and automatic frequency restoration reserves markets, *Appl. Energy* 298 (2021), <https://doi.org/10.1016/j.apenergy.2021.117267>.
- [38] C. Olk, D.U. Sauer, M. Merten, Bidding strategy for a battery storage in the German secondary balancing power market, *J. Energy Storage* 21 (2019) 787–800, <https://doi.org/10.1016/j.est.2019.01.019>.
- [39] K. Pandžić, I. Pavić, I. Andročec, H. Pandžić, Optimal battery storage participation in European energy and reserves markets, *Energies* (24) (2020) 13, <https://doi.org/10.3390/en13246629>.
- [40] L. Argiolas, M. Stecca, L.R. Elizondo, T.B. Soeiro, P. Bauer, Optimal battery energy storage dispatch in energy and frequency regulation markets while peak shaving an EV fast charging station, *IEEE Open Access J. Power Energy* (2022), <https://doi.org/10.1109/OAJPE.2022.3198553>.
- [41] I.M. Casla, A. Khodadadi, L. Soder, Optimal day ahead planning and bidding strategy of battery storage unit participating in Nordic frequency markets, *IEEE Access* 10 (2022) 76870–76883, <https://doi.org/10.1109/ACCESS.2022.3192131>.
- [42] A. Bowen, J. Engelhardt, T. Gabderakhmanova, M. Marinelli, G. Rohde, Battery buffered EV fast chargers on Bornholm: charging patterns and grid integration, in: 2022 57th International Universities Power Engineering Conference: Big Data and Smart Grids, UPEC 2022 - Proceedings, 2022, <https://doi.org/10.1109/UPEC55022.2022.9917690>.
- [43] Y. Vardanyan, F. Banis, S.A. Pourmousavi, H. Madsen, Optimal coordinated bidding of a profit-maximizing EV aggregator under uncertainty, in: 2018 IEEE International Energy Conference, ENERGYCON 2018, 2018, pp. 1–6, <https://doi.org/10.1109/ENERGYCON.2018.8398821>.
- [44] B. Tepe, J. Figgener, S. Englberger, D.U. Sauer, A. Jossen, H. Hesse, Optimal pool composition of commercial electric vehicles in V2G fleet operation of various electricity markets, *Appl. Energy* 308 (2022), <https://doi.org/10.1016/j.apenergy.2021.118351>.
- [45] M. Song, M. Amelin, X. Wang, A. Saleem, Planning and operation models for EV sharing community in spot and balancing market, *IEEE Trans. Smart Grid* 10 (6) (2019) 6248–6258, <https://doi.org/10.1109/TSG.2019.2900085>.
- [46] L. Meng, J. Zafar, S.K. Khadem, A. Collinson, K.C. Murchie, F. Coffele, G.M. Burt, Fast frequency response from energy storage systems - a review of grid standards, projects and technical issues, *IEEE Trans. Smart Grid* 11 (2) (2020) 1566–1581, <https://doi.org/10.1109/TSG.2019.2940173>.
- [47] J.O. Lee, Y.S. Kim, Novel battery degradation cost formulation for optimal scheduling of battery energy storage systems, *Int. J. Electr. Power Energy Syst.* 137 (2022), <https://doi.org/10.1016/j.ijepes.2021.107795>.
- [48] SMARD | Market data visuals. (n.d.). Retrieved November 1, 2022, from <https://www.smard.de/en/marktdaten?marketDataAttributes=%7B%22reSolution%22:%22hour%22,%22from%22:1661311069456,%22to%22:1662261469455,%22moduleIds%22:%5B18004368,18004369,18004370,18004351,18004374,18004373,18004371,18004372%5D,%22selectedCategory%22:null,%22activeChart%22:true,%22style%22:%22color%22,%22categorieModuleOrder%22:%7B%7D,%22region%22:%22DE%22%7D>.
- [49] Z. Wang, P. Jochem, W. Fichtner, A scenario-based stochastic optimization model for charging scheduling of electric vehicles under uncertainties of vehicle availability and charging demand, *J. Clean. Prod.* 254 (2020), <https://doi.org/10.1016/j.jclepro.2019.119886>.
- [50] N. Romero, K.van der Linden, G. Morales-España, M.M.de Weerdt, Stochastic bidding of volume and price in constrained energy and reserve markets, *Electric Power Syst. Res.* 191 (2021), <https://doi.org/10.1016/j.epsr.2020.106868>.
- [51] Fingrid - Fingridin avoin data. (n.d.). Retrieved September 14, 2023, from <https://data.fingrid.fi/en/organization/fingrid>.
- [52] View data published by RTE - RTE Services Portal. (n.d.). Retrieved September 14, 2023, from <https://www.services-rte.com/en/view-data-published-by-rte.html>.
- [53] Control reserve demand + activation - ancillary services - energy market - TransnetBW. (n.d.). Retrieved November 1, 2022, from <https://www.transnetbw.de/en/energy-market/ancillary-services/control-reserve-demand-activation>.
- [54] C. Li, L. Zhang, Z. Ou, Q. Wang, D. Zhou, J. Ma, Robust model of electric vehicle charging station location considering renewable energy and storage equipment, *Energy* 238 (2022), <https://doi.org/10.1016/j.energy.2021.121713>.
- [55] V.H. Bui, X.Q. Nguyen, A. Hussain, W. Su, Optimal sizing of energy storage system for operation of wind farms considering grid-code constraints, *Energies* (17) (2021) 14, <https://doi.org/10.3390/en14175478>.